An analytical approach to determining resonance in semi-closed convergent tidal channels

Cai, Huayang; Toffolon, M.; Savenije, Hubert H G

DOI
10.1142/S0578563416500091

Publication date
2016

Document Version
Final published version

Published in
Coastal Engineering Journal

World Scientific
www.worldscientific.com

JAPAN SOCIETY OF CIVIL ENGINEERS
COASTAL ENGINEERING COMMITTEE

Coastal Engineering Journal, Vol. 58, No. 3 (2016) 1650009 (37 pages)

DOI: 10.1142/S0578563416500091

An Analytical Approach to Determining Resonance in Semi-Closed Convergent Tidal Channels

Huayang Cai*

Institute of Estuarine and Coastal Research, School of Marine Sciences
Sun Yat-sen University, Guangzhou 510275, China

State and Local Joint Engineering Laboratory
of Estuarine Hydraulic Technology, Guangzhou 510275, China
Guangdong Provincial Key Laboratory of Marine Resources
and Coastal Engineering, Guangzhou 510275, China
**caihy7@mail.sysu.edu.cn*

Marco Toffolon

Department of Civil, Environmental and Mechanical Engineering
University of Trento, via Mesiano 77, Trento 38123, Italy
marco.toffolon@unitn.it

Hubert H. G. Savenije

Department of Water Management, Delft University of Technology
Stevinweg 1, P. O. Box 5048, Delft, 2600 GA, the Netherlands
h.h.g.savenije@tudelft.nl

Received 7 March 2016
Accepted 20 July 2016
Published 1 September 2016

An analytical model is used to investigate the resonant behavior in a semi-closed channel. The main integral quantities of the tidal wave are obtained by means of a linearized one-dimensional model as a function of three dimensionless parameters, representing

*Corresponding author.

cross-section convergence, friction and distance to the closed boundary. Arbitrary along-channel variations of width and depth are accounted for by using a multi-reach approach, whereby the main tidal dynamics are reconstructed by solving a set of linear equations satisfying the continuity conditions of water level and discharge at the junctions of the sub-reaches. We highlight the importance of depth variation in the momentum equation, which is not considered in the classical tidal theory. The model allows for a direct characterization of the resonant response and for the understanding of the relative importance of the controlling parameters, highlighting the role of convergence and friction. Subsequently, the analytical model is applied to the Bristol Channel and the Guadalquivir estuary. The proposed analytical relations provide direct insights into the tidal resonance in terms of tidal forcing, geometry and friction, which will be useful for the study of semi-closed tidal channels that experience relatively large tidal ranges at the closed end.

Keywords: Tidal resonance; amplification; tidal channel; analytical model.

1. Introduction

The tides in semi-closed estuaries, such as the Bay of Fundy, Gulf of California and Bristol Channel, are among the strongest in the world, offering potential for tidal energy generation by installation of tidal power barrages. It is therefore of practical importance as well as of theoretical interest to understand how the construction of a barrage would alter the tidal characteristics of the area and hence affect the aquatic environment and the potential use of water resources [Xia *et al.*, 2010; Zhou *et al.*, 2014]. In addition, it is important to understand the tidal response of an estuary to external changes (e.g. channel dredging, dam or weir construction, and sea level rise), which is closely related to navigation, design of coastal engineering works and estuarine environment.

Exceptionally high tidal ranges are primarily due to tidal resonance occurring when the natural period of oscillation in these systems is close to the dominant tidal period. Tidal wave amplification is also enhanced by convergence of channels [e.g. Friedrichs and Aubrey, 1994; Savenije, 2005, 2012]. Although the natural resonant period can be accurately determined by means of numerical models [e.g. Fong and Heaps, 1978; Greenberg, 1979; Zhong *et al.*, 2008; Cerralbo *et al.*, 2014; Liang *et al.*, 2014], the cause–effect relationships underlying the observed tidal behavior (e.g. the geometric effect on wave propagation and resonance) cannot be explicitly detected by single realizations of numerical runs. To this aim, analytical relationships are valuable tools that provide a direct insight. In addition, analytical models usually require a minimum amount of data, and provide explicit estimates of integral quantities (e.g. tidal amplitude, velocity amplitude, wave celerity and phase lag) without having the need to reconstruct them from temporal and spatial series.

Several solutions have been proposed in the context of one-dimensional (1D) models to provide insight into the propagation of a tidal wave in a semi-closed channel for different estuary shapes [e.g. Taylor, 1921; Hunt, 1964; Bennett, 1975; Robinson, 1980; Prandle and Rahman, 1980; Prandle, 1985; Rainey, 2009; van Rijn, 2011; Toffolon and Savenije, 2011; Winterwerp and Wang, 2013]. Most researchers

sought solutions described by functions that are valid for the entire estuary (we term this kind of approach as 'global'), often assuming a constant (linearized) friction term along the estuary. Taylor [1921] was one of the first to derive analytical solutions in semi-closed estuaries with width and depth varying linearly along the channel axis. He adopted a standing wave solution, which coincides with a frictionless estuary where there is no net transport of energy into the channel (since the water level and velocity are out of phase by 90°) and obtained the tidal amplitude as a Bessel function. Taylor's method was further developed by Bennett [1975] and Rainey [2009] by using the general solution of the tidal wave, including both incident and reflected waves, which enables the tidal wave to transport energy landward. However, their models did not take account of the frictional dissipation, resulting in a standing wave that is caused by the superposition of an incident and reflected wave. Later the frictional effect was included in an analytical solution by Robinson [1980], building on the works by Taylor [1921] and Bennett [1975]. The analytical solutions derived by Hunt [1964], Prandle and Rahman [1980], and Prandle [1985], who used different geometric schematizations, have large similarities with Robinson's approach with regard to linearization of the friction term and the exploitation of Bessel functions to describe the results. Similarly, van Rijn [2011], Toffolon and Savenije [2011] and Winterwerp and Wang [2013] proposed analogous analytical solutions for estuaries with convergent width and constant depth. Alebregtse *et al.* [2013] investigated the influence of a secondary channel on the resonance characteristics of the tidal wave in a main channel, but assumed a constant cross-section. Although Prandle and Rahman [1980] did take consideration of a variable depth in the continuity equation, they still assumed a constant friction factor (indicating a constant depth) in the momentum equation.

To gain additional insights into the vertical-longitudinal distribution of tidal currents, many other researchers derived two-dimensional (2D) width-averaged analytical solutions making use of perturbation analysis [e.g. Ianniello, 1979; Chernetsky *et al.*, 2010; Schuttelaars *et al.*, 2013]. Analogously, 2D depth-averaged models can be used to investigate the tidal dynamics in the longitudinal-transverse plane [e.g. Li and Valle-Levinson, 1999; Roos and Schuttelaars, 2011; Roos *et al.*, 2011]. On the basis of simplified geometry and flow characteristics, some researchers even derived three-dimensional (3D) analytical solutions to describe the tidal motions in a semi-closed channel [e.g. Winant, 2007; Jiang and Feng, 2014; Ensing *et al.*, 2015], or in a system of connected basins [e.g. Waterhouse *et al.*, 2011]. However, these models (2D or 3D) have to assume several simplifications in the geometrical description of the system and to include further parameterizations (e.g. for vertical eddy viscosity).

This study aims at providing an analytical tool to describe resonance in a semi-closed convergent channel, so we develop a 1D model as the simplest formulation that allows for reproducing the main tidal dynamics (i.e. a first-order solution). It has been shown that the analytical solutions to the 1D Saint Venant equations for tidal dynamics in an infinite channel can be cast in the form of a set of four

implicit equations for tidal damping, velocity amplitude, wave celerity (or speed) and phase lag in terms of two model parameters describing the friction and channel convergence [see Toffolon *et al.*, 2006; Savenije *et al.*, 2008; Cai *et al.*, 2012]. Similarly, here we demonstrate that the hydrodynamics in a semi-closed tidal channel can also be obtained by solving a set of implicit equations, which provide insights into the physical relation between the main tidal dynamics and model inputs (i.e. tidal forcing at the estuary mouth, length of the estuary, channel convergence and bottom friction).

In the next section, we present the model formulation. In Sec. 3, the analytical solutions for a single reach (with constant depth) is presented. Subsequently, we reformulate the solutions in implicit form using dimensionless parameters and account for along-channel variation of depth by using a multi-reach approach where the main tidal dynamics along the channel are reconstructed by solving a set of linear equations satisfying the internal boundary conditions at the junctions of these sub-reaches. In Sec. 4, the resonance behavior in a convergent semi-closed channel is presented. In Sec. 5, the analytical model is subsequently applied to the Bristol Channel and in the Guadalquivir estuary, distinguishing the main tidal constituents M_2 and S_2, and the resonance behavior in these two tidal channels is discussed. Finally, conclusions are drawn in Sec. 6.

2. Formulation of the Problem

2.1. *Geometry and governing equations*

We consider a semi-closed tidal channel of length L_e that is forced by one predominant tidal constituent with tidal frequency $\omega = 2\pi/T$, where T is the tidal period (e.g. $\sim$12.42 h for a M_2 tide). The water level is imposed at the seaward mouth of the channel, while a no-flux boundary condition is ensured at its head.

As the tidal wave propagates into the estuary, the signals of water level and velocity are characterized, respectively, by celerity c_A and c_V, amplitude η and υ, phase ϕ_A and ϕ_V. Figure 1 shows the geometry of the idealized tidal channel and a simplified picture illustrating the periodic oscillation of water level and velocity. Assuming that the flow is concentrated in a main rectangular cross-section, we seek solutions for water level and velocity for the case of convergent cross-sectional area $\overline{A}$ (an overbar denotes tidal average) and width $\overline{B}$, described by:

$$\overline{A} = \overline{A_0}\exp(-x/a), \qquad \overline{B} = \overline{B_0}\exp(-x/b), \tag{1}$$

where x is the longitudinal coordinate positive in landward direction, $\overline{A_0}$ and $\overline{B_0}$ are the values of cross-sectional area and width at the estuary mouth ($x = 0$), respectively, and a, b are their convergence lengths. It follows from the assumption of rectangular cross-section that the tidally averaged depth $\overline{h}$ is given by $\overline{h} = \overline{h_0}\exp(-x/d)$, where $\overline{h_0} = \overline{A_0}/\overline{B_0}$ is the tidally averaged depth at the estuary mouth and $d = ab/(b-a)$ is the convergence length of depth. The possible

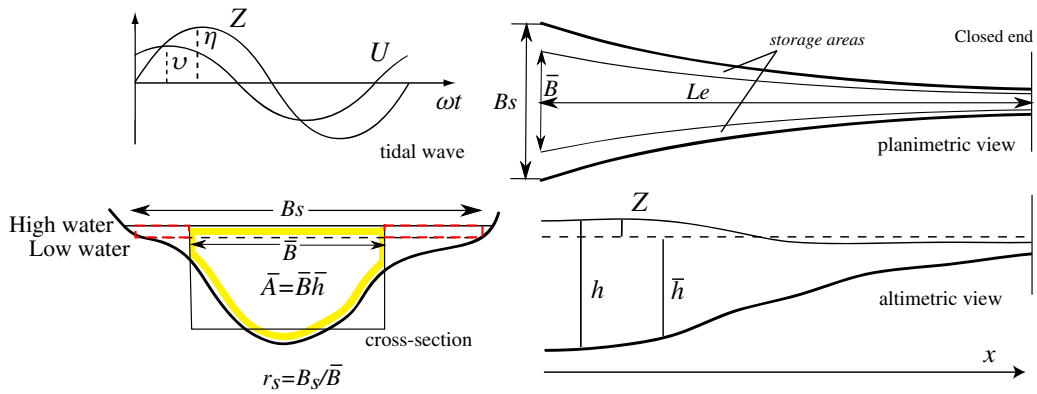

Fig. 1. Sketch of the tidal channel displaying the basic notation [after Savenije *et al.*, 2008].

influence of storage area (e.g. tidal flats) is quantified by the storage width ratio r_S, defined as the ratio of storage width B_S to tidally averaged width $\overline{B}$ (i.e. $r_S = B_S/\overline{B}$, see Fig. 1).

The cross-sectionally averaged continuity and momentum equations (one-dimensional Saint Venant equations) in a channel with gradually varying cross-section can be written as [e.g. Toffolon and Savenije, 2011]:

$$r_S \frac{\partial h}{\partial t} + U\frac{\partial h}{\partial x} + h\frac{\partial U}{\partial x} + \frac{hU}{\overline{B}}\frac{\mathrm{d}\overline{B}}{\mathrm{d}x} = 0, \tag{2}$$

$$\frac{\partial U}{\partial t} + U\frac{\partial U}{\partial x} + g\frac{\partial Z}{\partial x} + gj = 0, \tag{3}$$

where U is the cross-sectionally averaged velocity, Z the free surface elevation, $h = \overline{h} + Z$ is the depth, g the gravity acceleration, t is the time, and

$$j = \frac{U|U|}{K^2 h^{4/3}} \tag{4}$$

is the dimensionless friction term, with K the Manning–Strickler friction coefficient. The latter parameter describes the effective friction, including some factors of difficult quantification, in addition to the usual sediment roughness, like the additional drag resistance due to bed forms, the influence of suspended sediments [e.g. Winterwerp and Wang, 2013; Wang *et al.*, 2014], and the possible effect of lateral storage areas [e.g. Savenije, 2005, 2012]. Therefore, K is often considered as a parameter of the model to be calibrated against observations.

2.2. *Linearization and controlling parameters*

In order to pursue an analytical approach and obtain simple solutions, we linearize the governing equations by assuming that nonlinear products can be neglected in the governing equations [e.g. Toffolon and Savenije, 2011]. We linearize the friction term

by using a standard approach [Lorentz, 1926; Zimmerman, 1982] for the quadratic velocity and assuming a constant depth in the friction term (4), so that the linearized friction coefficient r is introduced:

$$gj = rU, \quad r = \frac{8}{3\pi}\frac{g\hat{v}}{K^2\overline{h}^{4/3}}. \tag{5}$$

In Eq. (5), $\hat{v}$ is a reference maximum velocity scale. The velocity amplitude v (strictly varying with x) is usually chosen as the typical velocity scale, i.e. $\hat{v} = v$. In general, an iterative procedure is needed to determine the correct friction factor r because v is an unknown parameter [e.g. Toffolon and Savenije, 2011; Roos and Schuttelaars, 2011].

The effect of nonlinearities can be important in many estuaries [e.g. Friedrichs and Aubrey, 1994; Alebregtse and de Swart, 2014], especially for large values of the amplitude-to-depth ratio. Moreover, overtides can be produced (such as M_4 from direct self-interaction of M_2) that produce a distortion of the wave shape. Although these effects can be directly reproduced by numerical models, here we neglect them following an analytical approach, which provides a complementary insight into the dynamics of resonance. In fact, mathematical relationships have a general validity that goes beyond the information gathered by a set of single numerical realizations.

We observe that linearized forms of Eqs. (2) and (3) can be combined to form a single, second-order differential equation for either Z or U. In principle, simple analytical solutions are only possible if the coefficients in the derived differential equation are constant, which implies a constant depth (and linearized friction) [e.g. van Rijn, 2011; Toffolon and Savenije, 2011; Winterwerp and Wang, 2013]. Otherwise, the solutions have to be formulated in terms of Bessel functions in order to account for variable depth in the continuity equation, but still assumed a constant friction factor in the momentum equation [e.g. Prandle and Rahman, 1980].

It was demonstrated by Toffolon and Savenije [2011] that the hydrodynamics in a semi-closed estuary are controlled by a few dimensionless parameters (defined in Table 1) that depend on geometry and external forcing but are independent of the resulting hydrodynamics (hence they are defined as independent): $\zeta_0 = \eta_0/\overline{h_0}$ the dimensionless tidal amplitude (at the seaward boundary), $\gamma = c_0/(\omega a)$ the estuary shape number (representing the effect of cross-sectional area convergence), χ_0 the friction number (describing the role of the frictional dissipation) and L_e^* the dimensionless estuary length (where the asterix indicates a dimensionless parameter), with η_0 the tidal amplitude at the seaward boundary, $c_0 = \sqrt{g\overline{h_0}/r_S}$ the reference wave celerity in a prismatic frictionless channel, and $L_0 = c_0T$ the tidal wavelength in a prismatic frictionless channel. It is noted that we adopt a slightly different length scale with respect to Toffolon and Savenije [2011], the ratio between them being 2π.

Table 1. Dimensionless parameters.

Independent	Dependent
Tidal amplitude at the mouth $\zeta_0 = \eta_0/\overline{h_0}$	Tidal amplitude $\zeta = \eta/\overline{h}$
Friction number at the mouth $\chi_0 = r_S c_0 \zeta_0 g/\left(K^2 \omega\, \overline{h_0}^{4/3}\right)$	Friction number $\chi = r_S c_0 \zeta g/\left(K^2 \omega \overline{h}^{4/3}\right)$
Estuary shape $\gamma = c_0/(\omega a)$	Velocity number $\mu = \upsilon/(r_S \zeta\, c_0)$
Estuary length $L_e^* = L_e/L_0$	Damping number for water level $\delta_A = c_0 \mathrm{d}\eta/(\eta\omega \mathrm{d}x)$
	Damping number for velocity $\delta_V = c_0 \mathrm{d}\upsilon/(\upsilon\omega \mathrm{d}x)$
	Celerity number for water level $\lambda_A = c_0/c_A$
	Celerity number for velocity $\lambda_V = c_0/c_V$
	Phase difference $\phi = \phi_V - \phi_A$

The main dependent (i.e. affected by the resulting hydrodynamics) dimensionless parameters are also presented in Table 1, and include: the actual values of dimensionless tidal amplitude ζ and friction number χ, the velocity number μ (the ratio of the actual velocity amplitude to the frictionless value in a prismatic channel), the celerity number for elevation λ_A and velocity λ_V (the ratio between the frictionless wave celerity in a prismatic channel and actual wave celerity), the amplification numbers for elevation δ_A and velocity δ_V (describing the rate of increase, δ_A (or δ_V) > 0, or decrease, δ_A (or δ_V) < 0, of the wave amplitudes along the estuary axis), and the phase difference between velocity and elevation $\phi = \phi_V - \phi_A$.

Different ways of presenting the linearized solution for tidal wave propagation are available in literature [e.g. van Rijn, 2011; Toffolon and Savenije, 2011; Winterwerp and Wang, 2013]. In the following analysis, we refer to the approach proposed by Toffolon and Savenije [2011], which is summarized in Appendix A.

3. Tidal Dynamics in Semi-Closed Channels

3.1. *Analytical solution*

Toffolon and Savenije [2011] derived simple implicit relationships for the main dependent dimensionless parameters (μ, δ_A, δ_V, λ_A, λ_V, ϕ) in a semi-closed estuary. In Appendix A, we elaborate these further and derive a new set of explicit relations as functions of δ_A and λ_A:

$$\delta_V = \gamma - \frac{\delta_A + \widehat{\chi}\lambda_A}{\delta_A^2 + \lambda_A^2}, \tag{6}$$

$$\lambda_V = \frac{\lambda_A - \widehat{\chi}\delta_A}{\delta_A^2 + \lambda_A^2}, \tag{7}$$

$$\mu^2 = \frac{\delta_A^2 + \lambda_A^2}{1 + \widehat{\chi}^2}, \tag{8}$$

$$\tan(\phi) = \frac{\delta_A + \widehat{\chi}\lambda_A}{\lambda_A - \widehat{\chi}\delta_A}, \tag{9}$$

where Eq. (8) is an implicit function of μ through the friction parameter $\widehat{\chi} = 8\mu\chi/(3\pi)$. Substituting $\widehat{\chi}$ into Eq. (8), a quadratic equation for μ^2 can be obtained, which gives the positive solution

$$\mu^2 = \frac{-1 + \sqrt{1 + 256\chi^2/(9\pi^2)(\delta_A^2 + \lambda_A^2)}}{128\chi^2/(9\pi^2)}. \tag{10}$$

Equations (6), (7), (9) and (10) allow us to directly estimate the main dependent parameters δ_V, λ_V, μ, ϕ as functions of the other two dependent parameters δ_A and λ_A. Thus, the problem of determining the specific tidal dynamics is reduced to finding the solution for δ_A and λ_A.

3.2. *Global solution*

The problem of specifying the parameters δ_A and λ_A in semi-closed channels can be easily solved within a global approach (i.e. considering uniform properties along the whole channel). These parameters can be obtained as a function of friction, convergence and along-channel location by the following equations (the derivation is provided in Appendix A):

$$\delta_A = \frac{\gamma}{2} - \Re\left\{\Lambda\left[1 - \frac{2}{1 + \exp(4\pi\Lambda L^*)\frac{\Lambda+\gamma/2}{\Lambda-\gamma/2}}\right]\right\}, \tag{11}$$

$$\lambda_A = \Im\left\{\Lambda\left[1 - \frac{2}{1 + \exp(4\pi\Lambda L^*)\frac{\Lambda+\gamma/2}{\Lambda-\gamma/2}}\right]\right\}, \tag{12}$$

where $\Lambda = \sqrt{\gamma^2/4 - 1 + i\widehat{\chi}}$, and $L^* = L_e^* - x^*$ is the distance to the closed end boundary.

The set of Eqs. (6)–(9), with the addition of (11) and (12), represents a new consistent analytical framework for understanding the tidal dynamics in a semi-closed system. Table 2 shows the analytical solutions for the general case as well as for some special cases: infinite channel length ($L^* \to \infty$), frictionless ($\chi = 0$, both with subcritical convergence, $\gamma < 2$, and supercritical convergence, $\gamma \geq 2$), and constant cross-section ($\gamma = 0$). In particular, if L^* approaches infinity, the set of Eqs. (6)–(9), (11) and (12) can be simplified and reduced to the analytical results

Table 2. New analytical framework for tidal hydrodynamics in a semi-closed tidal channel.

Cases	δ_A	λ_A	δ_V	λ_V	μ	$\tan(\phi)$
General	$\frac{\gamma}{2}-\Re\{\Lambda[1-\frac{2}{1+\exp(4\pi\Lambda L^*)\frac{\Lambda+\gamma/2}{\Lambda-\gamma/2}}]\}$	$\Im\{\Lambda[1-\frac{2}{1+\exp(4\pi\Lambda L^*)\frac{\Lambda+\gamma/2}{\Lambda-\gamma/2}}]\}$	$\gamma-\frac{\delta_A+\widehat{\chi}\lambda_A}{\delta_A^2+\lambda_A^2}$	$\frac{\lambda_A-\widehat{\chi}\delta_A}{\delta_A^2+\lambda_A^2}$	$\frac{\delta_A^2+\lambda_A^2}{1+\widehat{\chi}^2}$	$\frac{\delta_A+\widehat{\chi}\lambda_A}{\lambda_A-\widehat{\chi}\delta_A}$
Infinite length ($L^*\to\infty$)	$\frac{\gamma}{2}-\frac{4}{3\pi}\frac{\chi\mu}{\lambda_A}$	$\sqrt{1-\delta_A(\gamma-\delta_A)}$	$\frac{\gamma}{2}-\frac{4}{3\pi}\frac{\chi\mu}{\lambda_A}$	$\sqrt{1-\delta_A(\gamma-\delta_A)}$	$\frac{\cos(\phi)}{\lambda_A}=\frac{\sin(\phi)}{\delta_A-\gamma}$	$\frac{\delta_A-\gamma}{\lambda_A}$
Frictionless ($\chi=0$)						
Subcritical ($\gamma<2$)	$\frac{\sin(2\pi\alpha L^*)}{\cos(2\pi\alpha L^*-\theta)+\alpha/2}$	0	$\gamma-\frac{1}{\delta_A}$	0	δ_A	$\phi=\pi/2$
Supercritical ($\gamma\geq 2$)	$\frac{\gamma}{2}-\Lambda[1-\frac{2}{1+\exp(4\pi\Lambda L^*)\frac{\Lambda+\gamma/2}{\Lambda-\gamma/2}}]$	0	$\gamma-\frac{1}{\delta_A}$	0	δ_A	$\phi=\pi/2$
Constant cross-section ($\gamma=0$)	$-\Re\{\Lambda[1-\frac{2}{1+\exp(4\pi\Lambda L^*)}]\}$	$\Im\{\Lambda[1-\frac{2}{1+\exp(4\pi\Lambda L^*)}]\}$	$-\frac{\delta_A+\widehat{\chi}\lambda_A}{\delta_A^2+\lambda_A^2}$	$\frac{\lambda_A-\widehat{\chi}\delta_A}{\delta_A^2+\lambda_A^2}$	$\frac{\delta_A^2+\lambda_A^2}{1+\widehat{\chi}^2}$	$\frac{\delta_A+\widehat{\chi}\lambda_A}{\lambda_A-\widehat{\chi}\delta_A}$

for an infinite channel without reflected wave [Toffolon and Savenije, 2011]. The equations are provided in Appendix B, together with those obtained by Cai *et al.* [2012] using the 'envelope method'. For the frictionless case ($\chi = 0$), the detailed derivation of analytical solutions can be found in Appendix C.

The determination of the friction parameter $\widehat{\chi}$ requires the knowledge of the unknown value of μ (or υ), which is obtained iteratively [Toffolon and Savenije, 2011]. This can be done by the following procedure: (1) assume $\widehat{\chi} = \chi$ and compute $\mu = |V^*|$ using the analytical solutions presented in Sec. 3.1; (2) update $\widehat{\chi} = 8\mu\chi/(3\pi)$ and calculate a new value of μ; (3) repeat the process until it converges. The above process usually converges in a few steps.

3.3. *Multi-reach approach*

It is interesting to realize that the Eqs. (6)–(12) can be defined in each position x^* along the estuary. They consider the global dynamics along the reach of length L^* that remains to the head of the estuary. Interpreting them as a series of local relationships opens the possibility to obtain a simple description of the effect of the landward boundary on the wave properties along the estuary.

The tidal dynamics along estuary is affected by the longitudinal variation of the cross-section geometry (e.g. depth and friction) and by the reflected wave. Thus, we exploit a multi-reach approach [Toffolon and Savenije, 2011] that divides the whole estuary into sub-sections and solves a set of linear equations satisfying the internal boundary conditions (i.e. continuity of water level and velocity) at the junctions of the sub-reaches (see details in A.2). In principle, the proposed method is valid for arbitrary width and depth variations (not only exponential), even with strong longitudinal gradients.

To demonstrate the ability of the analytical model to reproduce the main tidal dynamics in a semi-closed estuary, we compared the analytical solution against a fully nonlinear one-dimensional numerical model [Toffolon *et al.*, 2006]. The numerical model uses an explicit MacCormack method and is second order accurate both in space and in time. Meanwhile, it exploits a Fourier analysis to extract the first tidal constituent (i.e. M_2) since we only focus on the behavior of the main wave component. As a test case, we consider a semi-closed estuary characterized by $\zeta_0 = 0.2$, $\overline{h_0} = 10\,\mathrm{m}$, $T = 12.42\,\mathrm{h}$, $b = 100\,\mathrm{km}$, $d = 160\,\mathrm{km}$, $K = 45\,\mathrm{m}^{1/3}\mathrm{s}^{-1}$, $r_S = 1$. Different channel lengths are considered between 20 km and 100 km. Figure 2 shows the analytically computed tidal amplitude and velocity amplitude compared with the numerical results: the analytical model is able to reproduce the fully nonlinear numerical results both qualitatively and quantitatively.

3.4. *Comparison among analytical models*

There exists many analytical theories for tidal hydrodynamics in a semi-closed tidal channel of various shape (constant, power or exponential) [e.g. Hunt, 1964; Ippen,

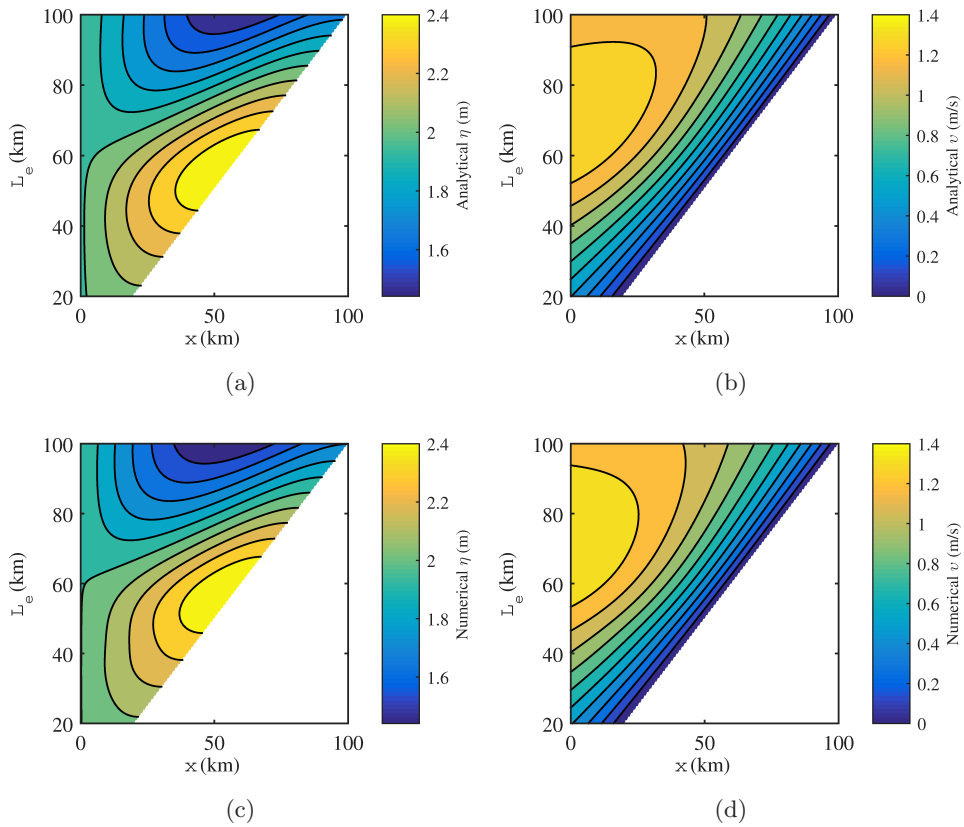

Fig. 2. Contour plot of the tidal amplitude η and the velocity amplitude υ in a semi-closed estuary with variable depth as a function of the position and of the estuary length, for given values of $\zeta_0 = 0.2$, $\overline{h_0} = 10\,\mathrm{m}$, $T = 12.42\,\mathrm{h}$, $b = 100\,\mathrm{km}$, $d = 160\,\mathrm{km}$, $K = 45\,\mathrm{m}^{1/3}\mathrm{s}^{-1}$, $r_S = 1$. Panels (a) and (b) present values of η and υ for the analytical model, while panels (c) and (d) present the numerical results.

1966; Prandle and Rahman, 1980; Souza and Hill, 2006; Toffolon and Savenije, 2011; van Rijn, 2011; Winterwerp and Wang, 2013]. The main differences among these solutions lie in the scaling method, the imposed boundary conditions, the geometric schematization and the way to linearize the friction term. It was demonstrated that all the linear analytical solutions for the tidal dynamics in an infinite tidal channel of exponentially converging width and constant depth [including those developed by Prandle, 1985; Friedrichs and Aubrey, 1994; Lanzoni and Seminara, 1998; Prandle, 2003; Friedrichs, 2010] are in principle identical since they are solving the same governing equations while exploiting a linearized friction term [Cai *et al.*, 2012; Cai, 2014]. Similar conclusions can be made for the case of a semi-closed tidal channel, as pointed out by Winterwerp and Wang [2013]. For instance, we note that the wavenumber defined in the paper of Winterwerp and Wang [2013] is a complex number (see their Eq. (10)), where the real part represents the dimensional wave number ω/c while the imaginary part represents the damping rate of tidal amplitude

$\mathrm{d}\eta/(\eta \mathrm{d}x)$. We observe that this dimensional complex wavenumber corresponds to our dimensionless complex number w_l^* $(l = 1, 2)$ defined by Eq. (A.11) in Appendix A (scaled by c_0/ω), except that the real part represents the damping factor δ_A while the imaginary part represents the celerity number λ_A.

However, most of the solutions used a constant friction factor r (see Eq. (5)), which suggests a constant maximum velocity scale and average depth in the linearized friction term. In our approach, the performance of the analytical model is improved by using an iterative procedure to correctly determine the maximum velocity scale and exploiting a multi-reach approach to account for variable geometry along the channel axis. We note that Prandle and Rahman [1980] used power functions to account for both width and depth variations in the continuity equation, but still assumed a constant friction factor in the momentum equation.

The analytical solution described by the set of implicit Eqs. (6)–(9), (11) and (12), is an extension of our previous solutions for an infinite tidal channel (see Appendix B). A special feature of this set of equations is that the relation between δ_V, λ_V, μ, ϕ, i.e. Eqs. (6)–(9), and δ_A, λ_A, can be interpreted as locally valid at each position (fixed x) along the channel, if the expressions (11) and (12) for the main dependent parameters δ_A, λ_A are taken as approximations for the dynamics in the landward part. The correct dynamics is reproduced by the multi-reach approach that accounts for along-channel variations of all geometrical and hydrodynamic variables (see previous Sec. 3.3).

3.5. *Tidal amplitude and wave celerity*

The main dimensionless parameters δ_V, λ_V, μ and ϕ are determined from Eqs. (6)–(10) as nonlinear functions of δ_A and λ_A. To illustrate the tidal dynamics, Fig. 3 presents an example of the solutions for δ_A and λ_A at the mouth of the estuary as a function of γ and L_e^*, for different values of χ.

Figures 3(a)–3(d) focus on δ_A, representing tidal wave amplification: negative values of δ_A refer to a longitudinal decrease of the amplitude (damping), while positive values refer to amplification. It is worth noting that in a semi-closed estuary the damping number δ_A varies significantly along the channel [e.g. Fig. 3(a)]. This is very different from the case of an infinite channel without wave reflection, where the condition $\delta_A = 0$ may be approximately valid for the entire channel, thus making it possible to define the ideal estuary condition where friction is balanced by channel convergence [Savenije *et al.*, 2008; Cai *et al.*, 2012]. For lower values of friction and convergence [χ and γ tending to zero, see Fig. 3(a)], resembling the case of a frictionless prismatic channel, a strong variation of δ_A occurs as a function of length L_e^* . The condition of no damping (indicated by the thick red lines) for a prismatic channel ($\gamma = 0$) corresponds with the usual resonant conditions at multiples of a quarter of the tidal wavelength (i.e. $L_e^* = j/4$ with $j = 1, 2, \ldots$). As will be clarified

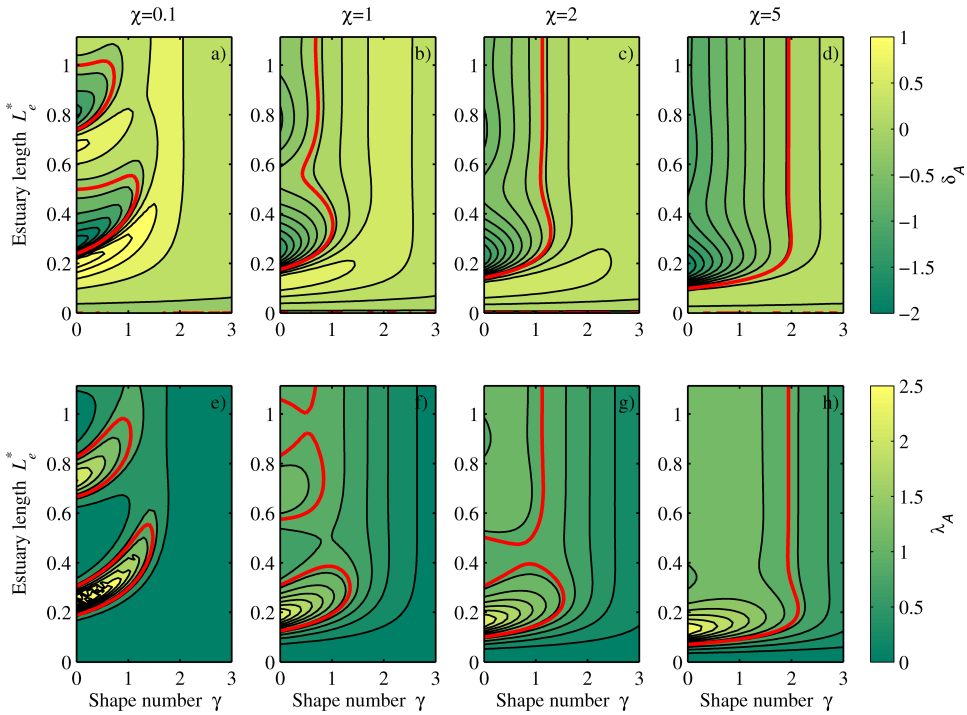

Fig. 3. (Color online) Contour plots of the damping number for tidal amplitude δ_A (a–d, > 0 amplification, < 0 damping) and celerity number for elevation λ_A (e–h, > 1 low celerity, < 1 high celerity) as a function of estuary shape number γ and dimensionless estuary length L_e^*, for different values of the friction number: (a, e) $\chi = 0.1$; (b, f) $\chi = 1$; (c, g) $\chi = 2$; (d, h) $\chi = 5$. The thick red lines indicate the values of $\delta_A = 0$ and $\lambda_A = 1$.

in the following section, even multiples (e.g. $L_e^* = 2/4, 4/4, \ldots$) correspond to antinodes, where the amplitude is maximum at the mouth. Conversely, odd multiples (e.g. $L_e^* = 1/4$, $L_e^* = 3/4$) correspond to nodes. At these lengths, slightly different values of L_e^* may produce a sudden change of sign of δ_A at the mouth with a sharp switch from positive to negative values. Moreover, the imposed amplitude at the mouth can be strongly amplified due to resonance. With increasing friction χ, the tidal wave damping increases (lower negative values of damping number δ_A), while convergence acts the other way around. When convergence is strong, the effect of the reflected wave becomes weaker and the tidal dynamics becomes more similar to an 'apparently standing wave' in an open ended estuary [Jay, 1991; Friedrichs and Aubrey, 1994; Savenije *et al.*, 2008]: the wave is not a formally standing wave generated by the superposition of incident and reflected waves; rather it is an incident wave that mimics a standing wave having a phase difference of $\phi = 90°$ between velocity and elevation and a wave celerity approaching infinity. The reason for this behavior is that in a strongly convergent estuary the reflected wave rapidly loses energy per unit width whereas the incident wave gains it. Friction intensifies this effect because the reflected wave loses its energy even quicker.

Figures 3(e)–3(h) show a similar picture for the celerity number λ_A. The higher its value, the lower is the wave celerity ($c = c_0/\lambda_A$). For straight channels with low friction [$\gamma \simeq 0$ in Figs. 3(a) and 3(e)] it is possible to recognize that the condition $\delta_A = 0$ corresponds to maximum or minimum values of λ_A, and hence of μ according to Eq. (10), with the maximum velocity occurring for $L_e^* = 1/4$. Such a behavior is a result of resonance, as will be elaborated in the next section. The influence of convergence tends to move the system toward a standing wave configuration, where the wave celerity approaches infinity ($\lambda_A = 0$). Figures 3(e)–3(h) also show the values of $\lambda_A = 1$ highlighted with thick red lines, which indicate that the wave celerity is the same as in a frictionless prismatic channel. On the other hand, the wave celerity decreases as friction increases. For large values of χ [e.g. Figs. 3(d) and 3(h)], we see that the pattern of the celerity number λ_A is similar to that of the damping number δ_A: $\lambda_A = 1$ almost corresponds to $\delta_A = 0$, which indicates that the system becomes similar to an infinite channel with negligible reflected wave.

It should be noted that the three independent parameters γ, χ and L^* are functions of frequency ω. Hence Fig. 3 shows not only the amplification of tidal amplitude and the wave celerity or speed, but also the frequency response at a specific position. Similar results were presented by Prandle and Rahman [1980], but they described the tidal amplification/damping by the ratio of tidal amplitude to that at a reference position (such as the head of the estuary) rather than the damping rate δ_A used in our approach.

4. Analysis of Resonance

4.1. *Response functions*

Previous studies on resonance behavior are mainly based on the response function of tidal amplitude in terms of location x and tidal frequency ω, where the maximum or minimum value corresponds to resonance and is achieved for given eigenvalue of ω (i.e. resonance frequency) and eigenvector representing the spatial structure of the resonance [e.g. Garrett, 1972; Ku *et al.*, 1985; Godin, 1988, 1993; Webb, 2012, 2013, 2014]. Garrett [1972] was one of the first to explore the resonance behavior in a tidal channel. He determined the resonant period of the Bay of Fundy based on the so-called 'Q factor' describing the energy dissipation near the resonance frequency in the response function. This method was further developed by Ku *et al.* [1985] including the nodal modulation of the M_2 tide. Subsequently, Godin [1988, 1993], building on the linearized St. Venant equations, derived the 'Q factor' as $\omega\overline{h}/r$, which is the inverse of the dimensionless friction parameter $\widehat{\chi}$ in our notation, i.e. $Q = 1/\widehat{\chi}$. Recently, Webb [2012, 2013, 2014] extended the analysis using complex values of tidal frequency and obtained new insights into understanding the tidal resonance. We realize that the previous studies exploiting 'Q factor' to determine the resonant period either used an oversimplified response function for tidal elevation [Garrett, 1972; Ku *et al.*, 1985] or did not account for the influence of channel convergence

[Godin, 1988, 1993] or required numerical results as inputs [Webb, 2012, 2013, 2014]. Conversely, in this paper, we analytically derived the amplified/damping rates of the tidal amplitude δ_A and the velocity amplitude δ_V for given channel convergence γ, bottom friction χ and distance to the closed end L^*, which can also be regarded as response functions of the system, since the independent parameters γ, χ and L^* are all functions of tidal frequency ω.

In the following sections, we investigate tidal resonance in a semi-closed estuary highlighting the importance of friction and channel convergence. The explicit consideration of these two elements is made possible for the first time thanks to the analytical formulation presented in the previous section. For sake of simplicity in presenting the results, here we focus on the cases with constant depth ($d \to \infty$, thus $a = b$) where the analytical solution of the system (6)–(9), (11) and (12) can be determined at each distance from the head of the estuary $L^* = L_e^* - x^*$. The same analysis could also be applied to a channel with a bottom slope ($a \neq b$) by means of the multi-reach approach presented in Sec. 3.3, which can be used for any type of along-channel depth variations.

Pure resonance only occurs in a frictionless case. Considering water level, nodes are those points where the tidal amplitude is zero ($\eta = 0$), while antinodes are those points where the tidal amplitude is maximum (hence $\delta_A = 0$). Their position is indicated by the dimensionless distances L^{*A}_{node} and L^{*A}_{antinode}, respectively, from the head of the estuary. Nodes and antinodes can also be defined considering the velocity amplitude. In this case we introduce the distance L^{*V}_{node} ($\upsilon = 0$) and L^{*V}_{antinode} ($\delta_V = 0$).

Nodes and antinodes are not properly defined in the frictional case. Real nodes ($\eta = 0$, $\upsilon = 0$) no longer exist, but virtual nodes can be defined as the position where the amplitude reaches its minimum value, although different from zero. Antinodes, however, can be identified by the condition $\delta_A = 0$ and $\delta_V = 0$, corresponding to maximum amplitude.

4.2. *Frictionless case*

The solution for the frictionless case is obtained by setting $\chi = 0$. This implies that $\lambda_A = 0$ and hence $\mu = \delta_A$ (see Appendix C), so the antinode for tidal amplitude coincides with the node for velocity amplitude ($L^{*A}_{\text{antinode}} = L^{*V}_{\text{node}}$). The cases of supercritical convergence ($\gamma \geq 2$) and subcritical convergence ($\gamma < 2$) need to be distinguished [Jay, 1991; Savenije *et al.*, 2008; Toffolon and Savenije, 2011]. Explicit solutions for the relevant parameters (δ_A, δ_V and μ) are derived from Eqs. (6), (8), (11) and (12) in Appendix C for both cases. The analysis of the position of nodes and antinodes confirms well-known results, but for the first time allows for an explicit consideration of the effect of convergence on resonance.

An example of the amplification produced by four different convergence rates is shown in Fig. 4. The local maximum values of η ($\delta_A = 0$) define the antinodes

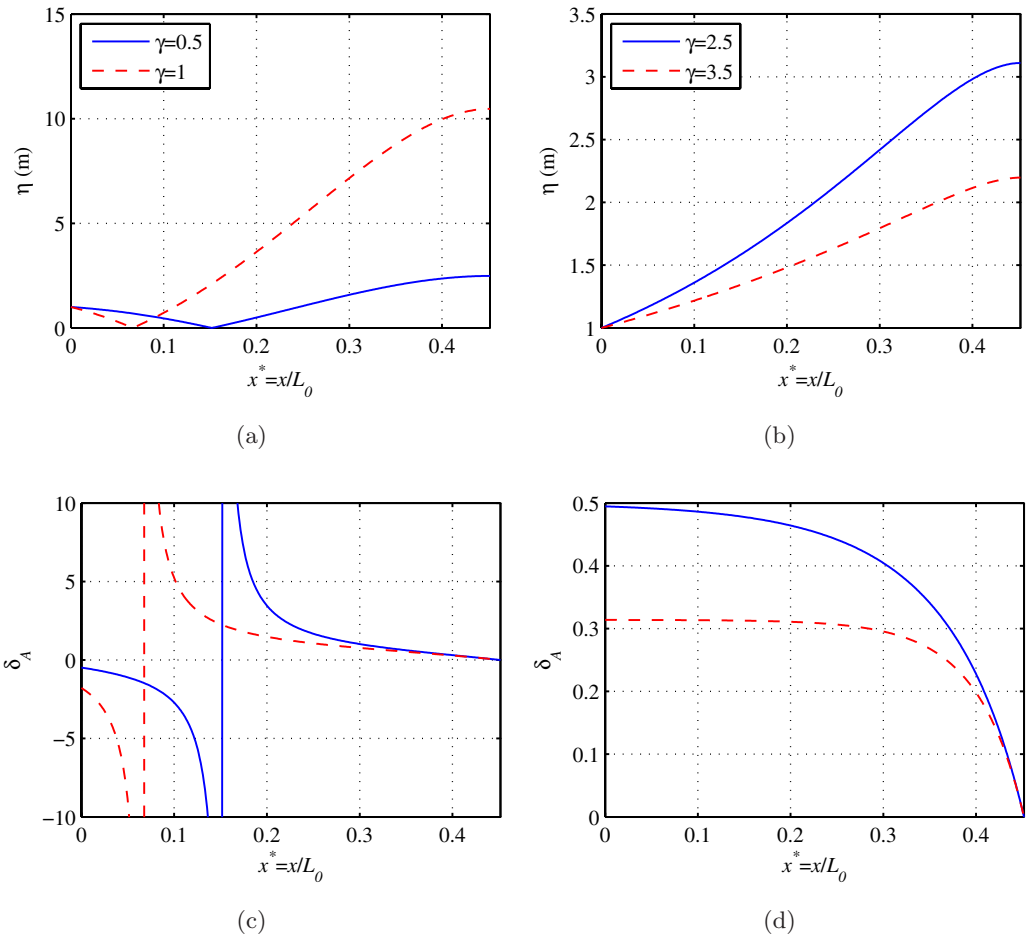

Fig. 4. Amplification for subcritical (a, c) and supercritical (b, d) convergence in a frictionless channel ($\chi = 0$) for different values of the estuary shape number: (a, b) longitudinal variation of tidal amplitude η; and (c, d) damping number δ_A. Other data: $T = 12.42$ h, $L_e = 200$ km, $\eta_0 = 1$ m, $\overline{h_0} = 10$ m, $r_S = 1$.

($\delta_A = 0$), while nodes occur where the amplitude vanishes ($\eta = 0$), a condition that corresponds to vertical asymptotes of δ_A with a change of its sign. Figure 5 summarizes the variation of the distance of the first node and antinode to the head as a function of estuary shape number γ.

In the subcritical range, when the estuary shape number γ increases (stronger channel convergence), the first node and antinode for tidal amplitude (and hence the node for velocity amplitude) move seaward until disappearing when they reach the total length of the estuary [Fig. 5 for $\gamma < 2$, see also Figs. 4(a) and 4(c)]. Only the first antinode for velocity amplitude moves landward. The tendency for $L^{*A}_{\text{node}} \to \infty$ is approached asymptotically for the critical convergence ($\gamma = 2$ in Fig. 5). The figure also shows that the well-known phenomenon that a frictionless channel resonates when it has a length of odd multiple of a quarter tidal wavelength

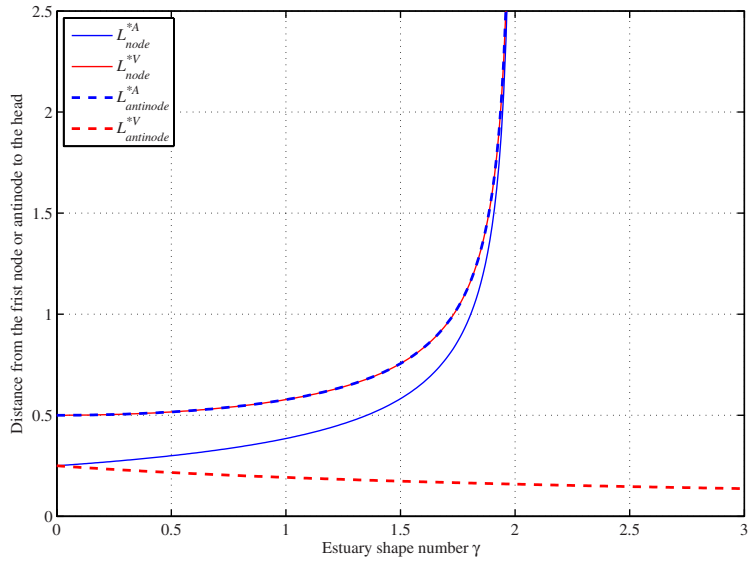

Fig. 5. The influence of convergence γ on the dimensionless distance from the position of the first node or antinode to the head in the frictionless case.

is only valid in a prismatic channel with a horizontal bed ($L^{*A}_{\text{node}} \to 0.25$ for $\gamma \to 0$ in Fig. 5).

Conversely, neither nodes nor antinodes for tidal amplitude exist for the supercritical case [Fig. 5 for $\gamma > 2$, see also Figs. 4(b) and 4(d)]. There only exists a single node for the velocity amplitude at the head of an estuary ($L^{*V}_{\text{node}} = 0$), as implied by the closed boundary at the head of the channel in any case. The position L^{*V}_{antinode} decreases as γ increases, hence bringing the maximum of velocity amplitude closer to the head of the estuary in strongly convergent estuaries. Interestingly, the analytical solution shows that the amplification decreases with increasing convergence [Fig. 4(d)] in the supercritical case, confirming the result found by Cai *et al.* [2012] for infinite channels.

Figure 6 shows a dimensional plot of the frequency response of the first tidal amplitude node in frictionless estuaries with different convergence length and depth. For prismatic channels ($b \to \infty$), we see that L^{A}_{node} approaches an asymptotic value which is one quarter of the tidal wavelength (i.e. $L_0/4$) for all frequencies. As the convergence length b decreases (larger γ), L^{A}_{node} tends toward infinity, thus making resonant conditions virtually impossible. This condition corresponds to the case where the estuary shape number γ tends toward 2 (i.e. the critical convergence for frictionless case). Indeed, a resonant behavior is manifested only for not too strong convergence, because the reflected wave quickly loses its energy if the width increases rapidly in the seaward direction. It is also interesting to note that the transition between an approximately constant value of L^{A}_{node} and the vertical asymptote occurs in a relatively limited range of value of the convergence length b.

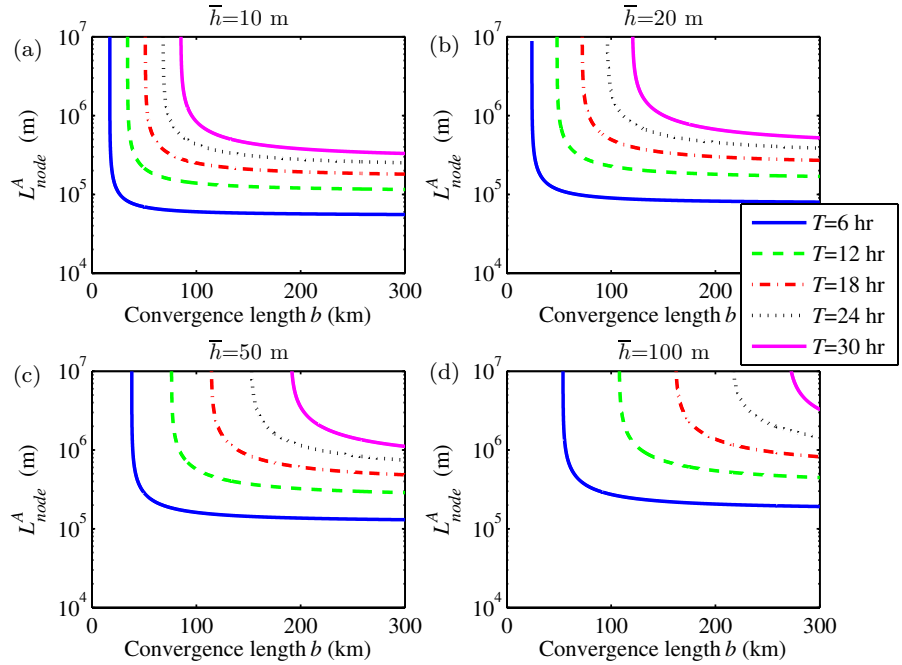

Fig. 6. The dimensional distance from the position L^A_{node} of the first tidal amplitude node to the head in a frictionless channel, as a function of convergence length b and tidal period T for different values of depth: (a) $\overline{h_0} = 10\,\text{m}$; (b) $\overline{h_0} = 20\,\text{m}$; (c) $\overline{h_0} = 50\,\text{m}$; and (d) $\overline{h_0} = 100\,\text{m}$.

4.3. *Frictional case*

In the frictional case ($\chi > 0$), an explicit analytical solution for the position of nodes and antinodes cannot be found, because it requires an iterative procedure. We can determine the distance of the first virtual tidal amplitude node to the head by varying the length of the estuary L_e^* and looking for a minimum value of the amplitude η at the mouth. Figure 7 shows how this distance, L^{*A}_{node}, varies as a function of γ and χ. We can see that the increase of friction moves the position of the first virtual node landward (shorter L^{*A}_{node}), while the channel convergence acts the other way around. Moreover, the resonance period $T_r = L_e/(c_0 L^{*A}_{\text{node}})$ is inversely proportional to L^{*A}_{node}, which suggests that friction tends to increase the resonance period of an estuary, while the channel convergence reduces it. In Fig. 7, the quarter wavelength case ($L^{*A}_{\text{node}} = 0.25$) is highlighted with a thick red line, which corresponds to a resonance period $T_{r0} = 4L_e/c_0$ in a prismatic channel with negligible friction ($\gamma = 0$, $\chi = 0$). If channel convergence is stronger than friction, the resonance period is less than T_{r0} (below the thick red line in Fig. 7); if friction is stronger than channel convergence, the resonant period is larger than T_{r0} (above the thick red line in Fig. 7); if they are balanced, the resonance period is equal to T_{r0} (the thick red line in Fig. 7).

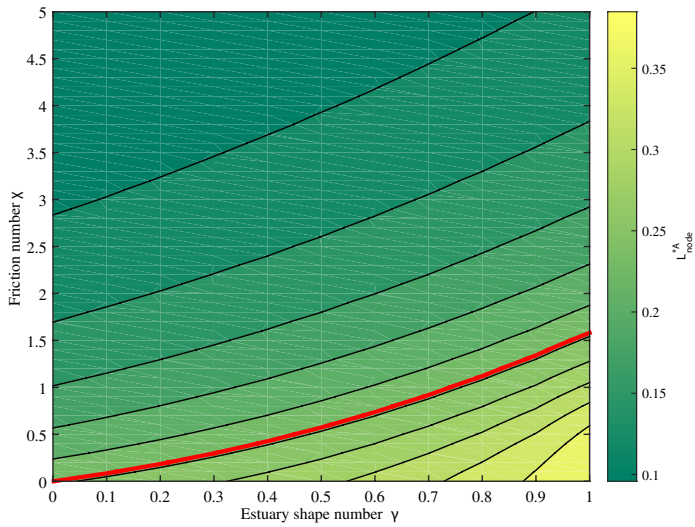

Fig. 7. (Color online) Contour plot of the distance of the first tidal amplitude node to the head L^{*A}_{node} in the γ–χ plane obtained by varying the length of the estuary L^*_e. The thick red line indicates the quarter wavelength case ($L^{*A}_{\text{node}} = 0.25$), which is the theoretical solution for a frictionless prismatic channel.

5. Tidal Reflection in the Bristol Channel and the Guadalquivir Estuary

5.1. *Application of the analytical model*

The analytical model presented in Sec. 3 has been applied to the Bristol Channel (U.K.) and the Guadalquivir estuary (Spain), where the geometric data (see Table 3) and tidal observations were obtained from Robinson [1980] and Diez-Minguito *et al.* [2012], respectively. The Bristol Channel is one of the largest estuaries in the UK, is characterized by a very large tidal range (whose simulation is challenging for a linearized model) and has repeatedly attracted scientific interest [e.g. Taylor, 1921; Rainey, 2009; Liang *et al.*, 2014]. The Guadalquivir estuary is located in the south-west part of Spain and has significant socio-economic importance and environmental

Table 3. Geometric characteristics and calibrated parameters used in studied estuaries.

Estuary	Mouth	a (km)	b (km)	d (km)	$\overline{B_0}$ (m)	$\overline{h_0}$ (m)	L_e (km)	K ($\text{m}^{1/3}\text{s}^{-1}$)	Correction coefficient f for S_2	r_S
Bristol channel	Ilfracombe	33.7	67	68	45110	33.1	129	54	3	1.2–1*
Guadalquivir	Port of Bonanza	60.3	65.5	760	795	7.1	103	46	5	1.5–1

Note: *A value of 1.2–1 means a linear reduction of the storage width ratio of 1.2–1 over the reach 0–129 km.

issues. The shape (width and depth) of the estuary has substantially changed due to intensive human interventions (such as dam constructions and periodical dredging for navigational purposes), which impacted the tidal dynamics and its flow regime. However, only few studies have investigated the evolution of hydrodynamics along the Guadalquivir estuary [e.g. Garcia-Lafuente *et al.*, 2012; Diez-Minguito *et al.*, 2012; Wang *et al.*, 2014].

The two case studies have been chosen to illustrate the performances of the analytical approach because they present similarities in the width convergence ratio, but are characterized by a significantly different response to resonance. The main geometrical characteristics of the two estuaries are collected in Table 3. The width convergence length b in both estuaries is similar, but the cross-sectional area convergence in the Bristol Channel ($1.5 < \gamma < 3.5$) is much stronger than that in the Guadalquivir estuary ($0.7 < \gamma < 0.9$) due to significant depth convergence in the Bristol Channel (depth convergence is defined referring to exponential variations for simplicity, but the method can be applied also to the real bathymetry). The comparison of these two different estuaries allows us to explore the geometric effect on the resonance behavior. Tides in both estuaries are dominated by the M_2 component (semidiurnal lunar tide, with a period of 12.42 h), with S_2 (semidiurnal solar tide, with a period of 12 h) being the second dominant tidal constituent.

The tidal amplitude and phase of elevation computed by the analytical solutions are presented in Fig. 8, along with M_2 and S_2 tidal observations. The correspondence with observations is good for M_2, while S_2 can be obtained only by adjusting the friction term. As explained in Appendix D, a correction factor f has been applied to the coefficient r in Eq. (5) to account for the interaction of S_2 with the dominant component:

$$r_{\text{new}} = fr = \frac{8}{3\pi}\frac{g\upsilon}{(K/\sqrt{f})^2\overline{h}^{4/3}}. \tag{13}$$

The correction factor f accounts for the actual friction experienced by the minor constituents. In fact, in a linearized model the velocity amplitude used as a reference in the linearized friction coefficient r is mainly determined by the principal tidal component [e.g. Pingree, 1983; Fang, 1987; Inoue and Garrett, 2007; Cai *et al.*, 2015], so r differs from constituent to constituent when considering a combined tidal signal.

One simple way to deal with this interaction is to modify the Manning–Strickler friction coefficient for the different constituents. We determined K for the M_2 tide by calibrating the model against observations filtered on this harmonic period, since M_2 is the dominant tidal constituent in both estuaries. Then, f has been calibrated with the observed S_2 tide. The values of K and f are presented in Table 3 along with the assumed storage width ratio r_S. We see that $f = 3$ has been used to reproduce the correct tidal dynamics for the secondary constituent S_2 in the Bristol Channel, while $f = 5$ is adopted in the Guadalquivir estuary. The factor f is always larger

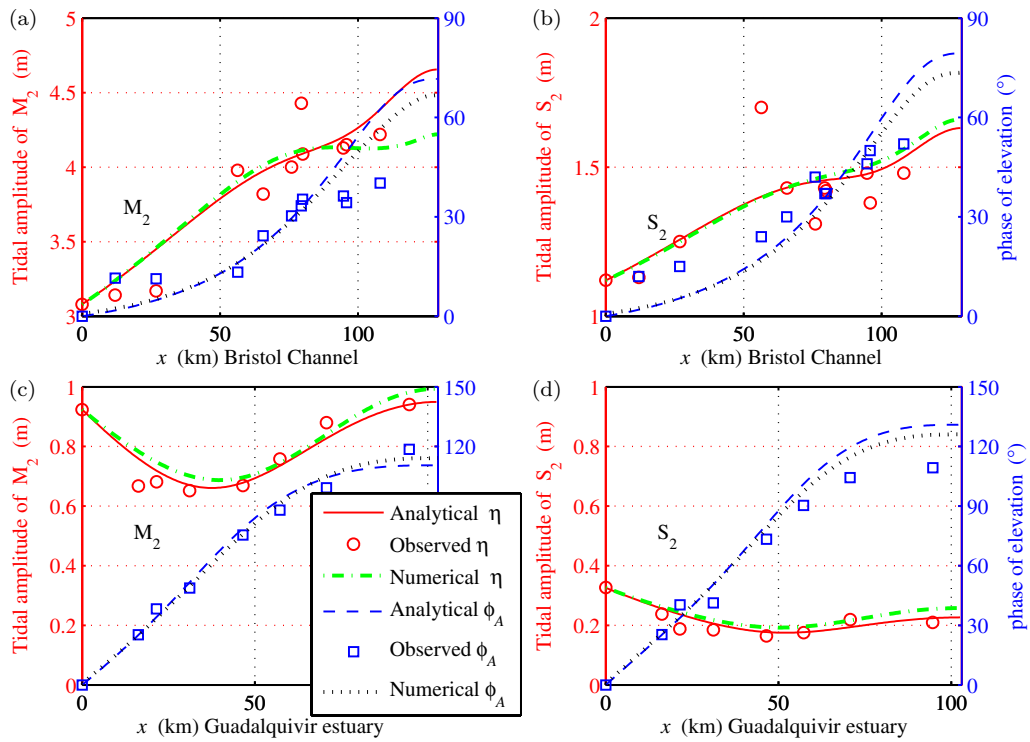

Fig. 8. Analytically and numerically calculated tidal amplitude and phase of elevation compared with observations for M_2 (a, c) and S_2 (b, d) in the Bristol Channel (a, b) and Guadalquivir estuary (c, d).

than unity, and grows for increasing ratios between the amplitudes of the dominant and the secondary tidal components (see Appendix D).

Note that the analysis presented in Diez-Minguito *et al.* [2012] with regard to the Guadalquivir estuary, based on a standard harmonic analysis, provides results of wave propagation over a complete frequency range, while here we mainly focus on the dominant semi-diurnal components (i.e. M_2 and S_2) aiming to reproduce the main tidal dynamics along the channel by means of an analytical method. For further details of the wave propagation of other tidal constituents, readers can refer to Diez-Minguito *et al.* [2012].

To examine the performance of analytical model, in Fig. 8 we also present numerical results obtained using the 1D numerical model [see Toffolon *et al.*, 2006] making use of the same friction coefficients as in the analytical model. For the weaker tidal constituent S_2, it directly follows from (13) that the corrected friction coefficient is expressed as $K/\sqrt{f}$. The agreement between analytical and numerical results is satisfactory since the analytical solution is able to both qualitatively and quantitatively reproduce the numerical results in the two estuaries. The difference between the numerical and analytical M_2 results near the upstream boundary of the Bristol

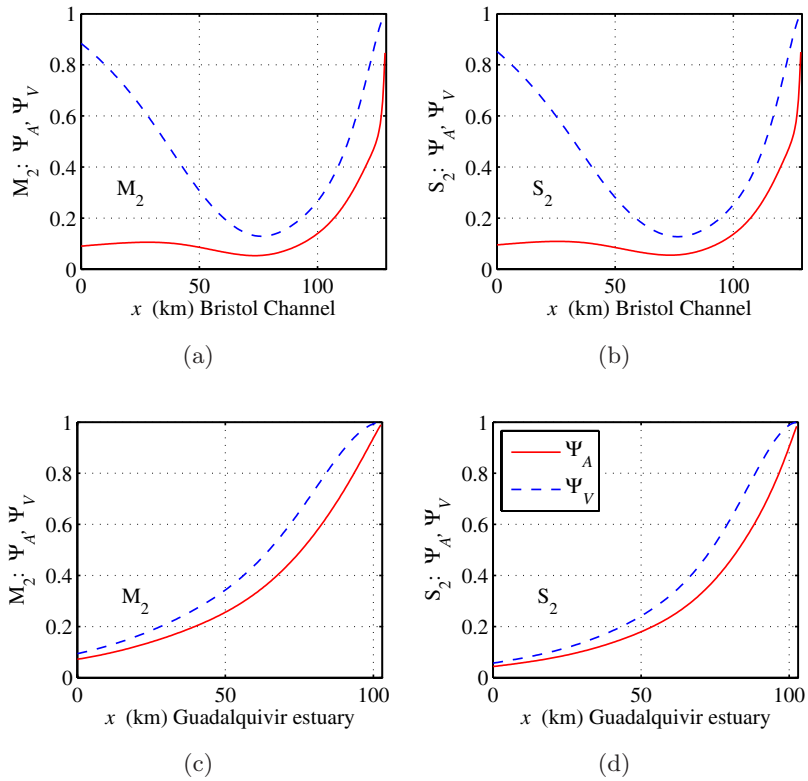

Fig. 9. Longitudinal variation of the reflection coefficients Ψ_A and Ψ_V for M_2 (a, c) and S_2 (b, d) tides in the Bristol Channel (a, b) and Guadalquivir estuary (c, d).

Channel [see Fig. 8(a)] is somewhat unexpected, but probably due to the difficulty of the Fourier separation near the upstream boundary.

Figure 9 shows the analytically computed longitudinal variation of the reflection coefficients for tidal amplitude Ψ_A and velocity amplitude Ψ_V (please refer to Appendix A for the precise definition) for both M_2 and S_2 tidal constituents in these two estuaries. The maximum reflection is of course reached at the closed end. We also note that the reflection for the velocity amplitude is bigger than that for the tidal amplitude ($\Psi_V > \Psi_A$) in both estuaries, but especially in the Bristol Channel near the mouth. In this estuary, the minimum of the reflection occurs approximately at 76 km from the mouth. Conversely, in the Guadalquivir estuary both reflection coefficients increase continuously along the estuary.

It is worth noting that Diez-Minguito *et al.* [2012] adopted a linear analysis using a least squares fitting technique to derive the reflection coefficient for different tidal constituents. However, their method requires a simplified estuarine system where both the effects of friction and convergence are negligible. From Figs. 9(c) and 9(d), we observe that the reflection coefficient of semi-diurnal tides (M_2 and S_2) near the dam ($x = 88$ km, a distance of 15 km from the close end) is around 0.7,

which is much larger than the value 0.4 estimated in Sec. 4 in Diez-Minguito *et al.* [2012]. The deviation might be due to their assumption that a standard dispersion relationship between frequency and wavenumber (i.e. the one obtained for gravity waves in an infinite domain) holds also close to the boundary, while in our analysis the wavenumber is computed in each position along the channel and may vary significantly. On the other hand, for a greater distance of 70 km from the closed end (i.e. $x = 47$ km), the reflection coefficient predicted by Diez-Minguito *et al.* [2012] is very close to the analytical result ($\sim$0.25 in both cases). The good correspondence at this position suggests that the dispersion relationship becomes more valid sufficiently far from the boundary. The proposed analytical method can be regarded as a useful tool to further understand the tidal reflection along the Guadalquivir estuary.

5.2. *Resonance behavior*

It is of interest to explore the resonance period in a semi-closed estuary since it provides insights into the ability of an estuary to resonate in the presence of friction and channel convergence. The analytical model allows for considering the separate effect of the different tidal constituents in a computationally very efficient way and in a wide parameter space. Thus, it can be considered as a complementary approach to numerical models, which provide more accurate results, including nonlinear interactions, but are concerned with single realizations and yield aggregate dynamics, from which it is necessary to extract the information on single constituents. Moreover, numerical models do not allow for recognizing the separate effect of direct and reflected waves propagating along the channel.

In the present analysis, the condition for tidal resonance to occur in a channel is that the tidal amplitude at the head reaches its maximum value. Figures 10 and 11 show how the main tidal parameters (including tidal amplitude η, phase difference ϕ between elevation and velocity, incident tidal amplitude η_I and reflected tidal amplitude η_R) develop in response to tidal forcing with period varying between 1 and 40 h (with 0.5 h interval) at the estuary mouth in the Bristol Channel and the Guadalquivir estuary, respectively. We assume that the tidal forcing at the ocean boundary is constant and equal to the amplitude of the examined tidal component.

In the Bristol Channel, the tidal amplitude at the estuary head reaches a maximum value when T is approximately 12 h [i.e. resonance period, see Fig. 10(a)], which is close to the semi-diurnal periodicity. In Fig. 10(b), we see how the phase varies along the estuary axis with forcing of different periods. At the resonant period the phase reduces to a minimum value (i.e. 63°) around $x = 58$ km before it increases until 90° at the head of the estuary. The contributions of the incident and reflected waves to the tidal amplitude can be found from Figs. 10(c) and 10(d). The amplitude of the incident wave increases until a maximum value is reached around $x = 68$ km [Fig. 10(c)], which is due to the fact that the geometric amplification arising channel

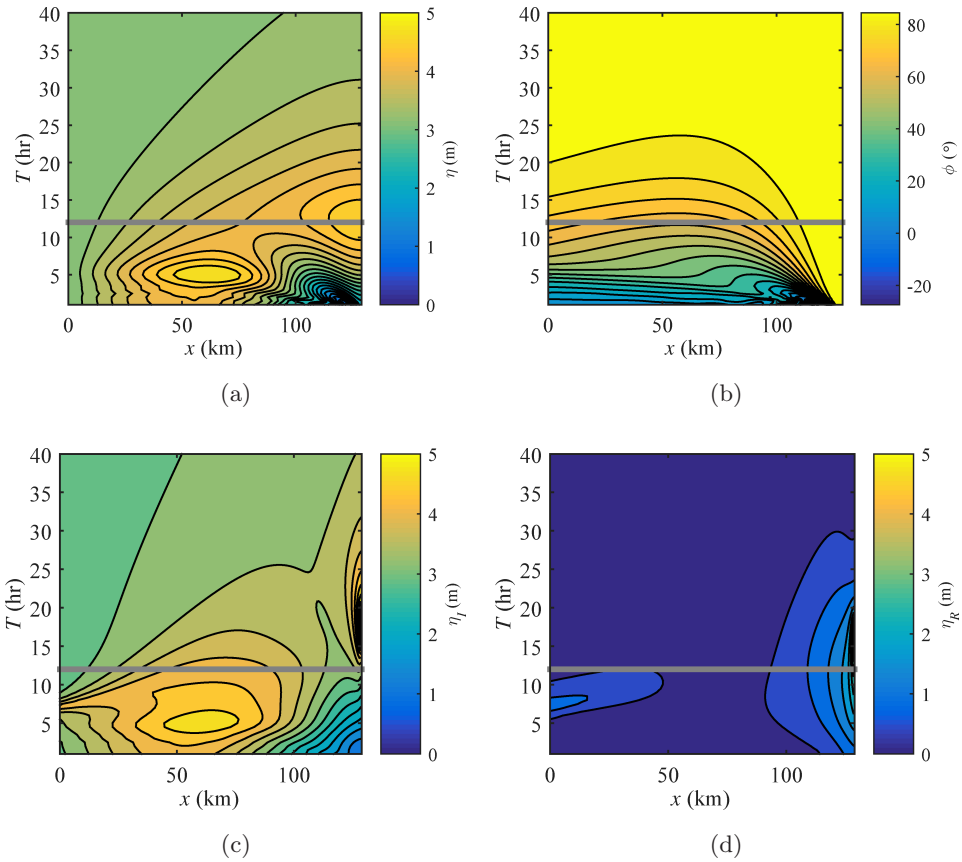

Fig. 10. Contour plot of the main parameters in the Bristol Channel as a function of distance x and tidal period T: (a) tidal amplitude; (b) phase difference between elevation and velocity; (c) incident tidal amplitude; and (d) reflected tidal amplitude. The gray line represents the longitudinal development at the resonance period (i.e. 12 h) when the tidal amplitude at the head of the estuary is largest.

convergence is stronger than frictional damping. On the other hand, we see that the amplitude of the reflected wave generally decays as it propagates from the head to the estuary mouth [Fig. 10(d)] due to the damping introduced by channel divergence and friction. In Figs. 10(c) and 10(d), we also note that the amplitude of the incident wave at the estuary head reaches its maximum at a tidal period of 17 h, while it is 16.5 h for the reflected wave, which is different from the resonance period of 12 h. This is due to the phase difference between incident and reflected waves.

Figure 11 shows a similar picture for the Guadalquivir estuary, which tends to resonate at a period of 35 h (when tidal amplitude at the estuary head is the largest), and not close to the semi–diurnal periodicity nor the diurnal periodicity [Fig. 11(a)]. At semi-diurnal periodicity, the tidal amplitude reduces to its lowest value around $x = 50$ km, before the geometric amplification increases it further upstream. The phase at both semi-diurnal and diurnal periodicities is increased along the estuary

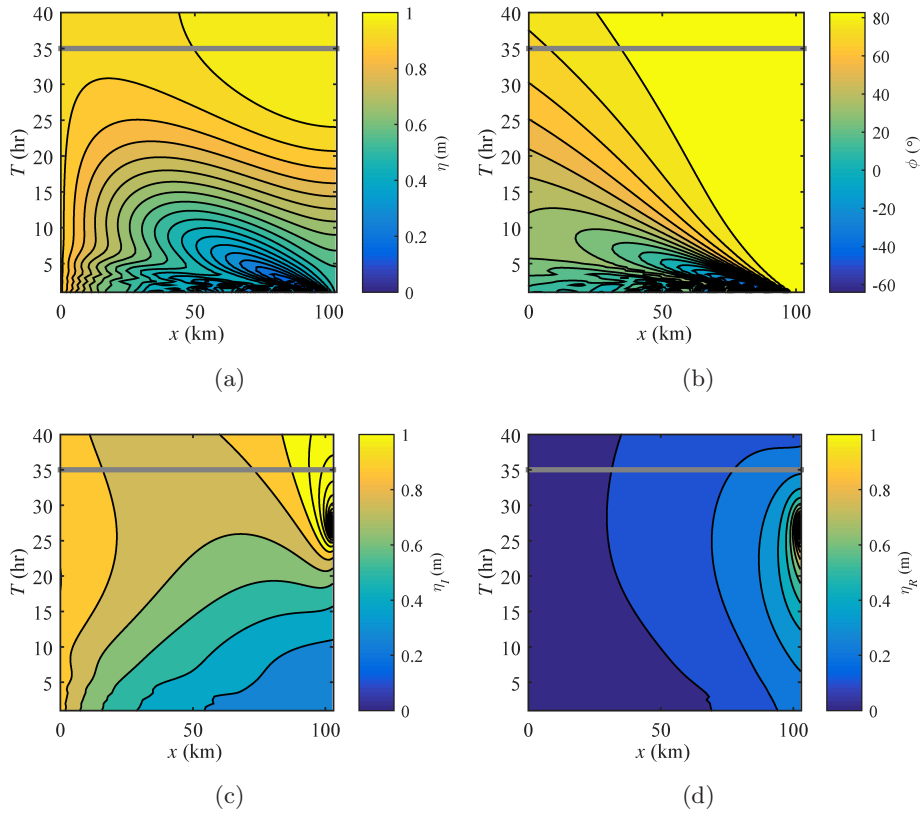

Fig. 11. Contour plot of the main parameters in the Guadalquivir estuary as a function of distance x and tidal period T: (a) tidal amplitude; (b) phase difference between elevation and velocity; (c) incident tidal amplitude; and (d) reflected tidal amplitude. The gray line represents the longitudinal development at the resonance period (i.e. 35 h) when the tidal amplitude at the head of the estuary is largest.

axis until a phase of 90° is reached at the head of the estuary [Fig. 11(b)]. Both the incident and reflected waves make considerable contributions to the tidal amplitude [Figs. 11(c) and 11(d)]. At the resonant period, the amplitude of the incident wave increases in landward direction while that of the reflected wave decreases in the opposite direction [Fig. 11(c)]. In contrast, the behavior of the incident wave at semi-diurnal periodicity is opposite, i.e. decreasing from the mouth to the head. This phenomenon is related to the relative importance of convergence (indicated by γ) and frictional dissipation (represented by χ), since both γ and χ are linearly proportional to the tidal period (see Table 1). The behavior of the reflected wave is similar to that in the Bristol Channel, i.e. decaying in seaward direction.

6. Conclusions

The analytical solution for linearized one-dimensional tidal hydrodynamics developed by Toffolon and Savenije [2011] has been used to explore the resonance

behavior in semi-closed channels with variable width and depth. We have reformulated the analytical solution in terms of equations involving the main tidal wave parameters (amplitude, amplification, celerity, phase lag). The resulting set of equations forms a consistent theoretical framework for describing the tidal wave propagation and its reflection due to a close end (e.g. tidal barrage or weir), as a function of two externally defined dimensionless parameters (representing friction and cross-section convergence) and of the longitudinal coordinate (distance to the closed boundary). To account for the depth variations along the channel, we exploited a multi-reach technique, subdividing the total channel in multiple reaches and reconstructing the tidal dynamics by solving a set of linear equations satisfying the continuity conditions of water level and discharge at junctions of these subreaches. Unlike the classical tidal theory [e.g. Prandle and Rahman, 1980] assuming an effective drag coefficient (indicating a constant depth and velocity amplitude in the friction term), the proposed model allows for taking account of depth variation in the momentum equation, which is important when longitudinal depth variation is notable.

We have highlighted the importance of channel convergence on the resonant behavior both with and without friction. Explicit analytical expressions for the positions of nodes and antinodes have been derived for the water level and velocity when friction is negligible. For the frictional case, these positions can only be obtained numerically and represented in graphical form because an explicit solution cannot be derived. However, in those cases where a numerical solution of the set of equations for the tidal parameters is needed, the computational effort is absolutely negligible with respect to complete numerical simulations.

The analytical approach relies on several assumptions, starting from the linearization of the governing Saint Venant equations, and hence the results cannot be as accurate as those of fully nonlinear numerical simulations. Nonetheless, the analytical approach has some important advantages with respect to numerical runs. First, equations are written in terms of clearly identifiable integral quantities (e.g. amplitude, phase, damping) that otherwise have to be reconstructed from numerical simulations by means of suitable algorithms. Second, wide ranges in the parameter space can be considered, while a general interpretation of the tidal behavior can be obtained from numerical simulations only by the sum of a large number of single runs. Third, the individual effects of tidal constituents that do not result from direct harmonic interactions (i.e. that are not overtides) can be analyzed separately. Fourth, the specific contribution of the direct and reflected waves to resonance can be explicitly detected, which is not straightforward from numerical runs. These considerations make the analytical approach a complementary tool that can support specific numerical runs by providing the general picture, and by giving physical hints for the interpretation of the usually complex dynamics of numerical results.

The analytical model has been applied to the Bristol Channel and the Guadalquivir estuary considering the dominant tidal component (M_2) and a weaker

secondary constituent (S_2). A correction to the linearized friction term for the secondary component was used to account for the quadratic total velocity. The analysis shows that the Bristol Channel tends to resonate close to semi-diurnal period (12 h), while the Guadalquivir estuary at a period of 35 h.

The proposed analytical approach represents a new consistent analytical framework for understanding the tidal hydrodynamics in semi-closed tidal channels, in which the relations among the main tidal dynamics can be described by using a set of six implicit equations (see Table 2). The merit of the method is that it provides direct insights into the tidal resonance in terms of external parameters (i.e. tidal forcing, geometry, friction), which is useful for the study of tidal channels that experience relatively large tidal ranges at the closed end.

Appendix A. Linearized Solution and Derivation of the Parameters for a Semi-Closed Channel

A.1. *Global approach*

In this appendix we follow the approach proposed by Toffolon and Savenije [2011], who linearized the continuity and momentum Eqs. (2) and (3) and imposed the following structure to the two unknowns, water level and velocity:

$$Z = \zeta_0 \overline{h_0}[A^* \exp(\mathrm{i}\omega t) + \mathrm{Cc}]/2, \quad U = r_S \zeta_0 c_0 [V^* \exp(\mathrm{i}\omega t) + \mathrm{Cc}]/2, \tag{A.1}$$

where A^* and V^* are unknown complex functions (Cc represents the complex conjugate of the preceding term) varying along the dimensionless coordinate $x^* = x/L_0$:

$$A^* = a_1^* \exp(2\pi w_1^* x^*) + a_2^* \exp(2\pi w_2^* x^*), \tag{A.2}$$

$$V^* = v_1^* \exp(2\pi w_1^* x^*) + v_2^* \exp(2\pi w_2^* x^*), \tag{A.3}$$

where a_1^*, a_2^*, v_1^*, v_2^*, w_1^*, and w_2^* are unknown complex variables to be determined by the boundary conditions.

The first term on the right-hand side of Eq. (A.2) represents a wave traveling seaward (i.e. reflected wave), while the second term represents a wave traveling landward (i.e. incident wave). As a result, the reflection coefficients Ψ_A for tidal amplitude (the ratio of the amplitude of the reflected to incident wave) and Ψ_V for velocity amplitude are given by:

$$\Psi_A = \left|\frac{a_1^*}{a_2^*}\right|, \quad \Psi_V = \left|\frac{v_1^*}{v_2^*}\right|. \tag{A.4}$$

The analytical solutions for the tidal amplitudes and phases are given by:

$$\eta = \zeta_0 \, \overline{h_0} \, |A^*|, \quad \upsilon = r_S \, \zeta_0 \, c_0 \, |V^*|, \tag{A.5}$$

$$\tan(\phi_A) = \frac{\Im(A^*)}{\Re(A^*)}, \quad \tan(\phi_V) = \frac{\Im(V^*)}{\Re(V^*)}, \tag{A.6}$$

with $\Im(A^*)$ representing the imaginary part of A^* and $\Re(A^*)$ the real part. Then, the dependent dimensionless parameters (defined in Table 1) can be computed by the following equations:

$$\mu = |V^*|, \quad \phi = \phi_V - \phi_A, \tag{A.7}$$

$$\delta_A = \Re\left(\frac{1}{A^*}\frac{\mathrm{d}A^*}{\mathrm{d}x^*}\right), \quad \delta_V = \Re\left(\frac{1}{V^*}\frac{\mathrm{d}V^*}{\mathrm{d}x^*}\right), \tag{A.8}$$

$$\lambda_A = \Im\left(\frac{1}{A^*}\frac{\mathrm{d}A^*}{\mathrm{d}x^*}\right), \quad \lambda_V = \Im\left(\frac{1}{V^*}\frac{\mathrm{d}V^*}{\mathrm{d}x^*}\right). \tag{A.9}$$

Toffolon and Savenije [2011] also derived the solution for the particular case of a closed-end channel. The analytical solutions A^* and V^* can be obtained using

$$a_1^* = \left[1 + \exp\left(4\pi\Lambda L^*\right)\frac{\Lambda + \gamma/2}{\Lambda - \gamma/2}\right]^{-1}, \quad a_2^* = 1 - a_1^*, \tag{A.10}$$

$$v_1^* = \frac{-i\,a_1^*}{\Lambda - \gamma/2}, \quad v_2^* = \frac{i(1 - a_1^*)}{\Lambda + \gamma/2}, \quad w_1^* = \gamma/2 + \Lambda, \quad w_2^* = \gamma/2 - \Lambda, \tag{A.11}$$

where

$$\Lambda = \sqrt{\gamma^2/4 - 1 + i\widehat{\chi}}, \quad \widehat{\chi} = \frac{8}{3\pi}\mu\chi, \tag{A.12}$$

and $L^* = L_e^* - x^*$ is the distance to the closed end boundary.

Within a single-reach approach, further elaboration of the above equations yields

$$\delta_A - i\lambda_A = \left.\frac{1}{A^*}\frac{\mathrm{d}A^*}{\mathrm{d}x^*}\right|_{x^*=0} = \frac{\gamma}{2} - \Lambda\left[1 - \frac{2}{1 + \exp(4\pi\Lambda L^*)\frac{\Lambda+\gamma/2}{\Lambda-\gamma/2}}\right]. \tag{A.13}$$

Equation (A.13), expressed in complex notation, can be separated into its real and imaginary parts, leading to Eqs. (11) and (12) in the main text.

Similarly, we can derive that

$$\begin{aligned}\delta_V - i\lambda_V &= \left.\frac{1}{V^*}\frac{\mathrm{d}V^*}{\mathrm{d}x^*}\right|_{x^*=0} = \gamma + \frac{1 - i\widehat{\chi}}{-\gamma/2 + \Lambda(1 - 2a_1^*)} \\ &= \gamma + \frac{1 - i\widehat{\chi}}{-\delta_A + i\lambda_A} = \gamma - \frac{\delta_A + \widehat{\chi}\lambda_A}{\delta_A^2 + \lambda_A^2} + i\frac{\lambda_A - \widehat{\chi}\delta_A}{\delta_A^2 + \lambda_A^2}.\end{aligned} \tag{A.14}$$

By separately equating the real and imaginary parts of the above equation, we have

$$\delta_V = \gamma - \frac{\delta_A + \widehat{\chi}\lambda_A}{\delta_A^2 + \lambda_A^2}, \quad \lambda_V = \frac{\lambda_A - \widehat{\chi}\delta_A}{\delta_A^2 + \lambda_A^2}. \tag{A.15}$$

Since $V^*\big|_{x^*=0} = \upsilon_1^* + \upsilon_2^*$, we can also derive that

$$\mu^2 = |V^*|^2 = \left|\frac{-\gamma/2 + \Lambda(1-2a_1^*)}{\widehat{\chi}+i}\right|^2$$
$$= \left|\frac{1}{-i(\delta_V - \gamma + i\lambda_V)}\right|^2 = \frac{1}{(\delta_V^2-\gamma)^2+\lambda_V^2} = \frac{\delta_A^2+\lambda_A^2}{1+\widehat{\chi}^2}. \tag{A.16}$$

It follows from (A.16) that

$$\tan(\phi_V) = \frac{\Im(V^*)}{\Re(V^*)} = \frac{\gamma-\delta_V}{\lambda_V} = \frac{\delta_A + \widehat{\chi}\lambda_A}{\lambda_A - \widehat{\chi}\delta_A}. \tag{A.17}$$

We impose that the phase ϕ_A is zero at the seaward boundary of each reach by locally shifting the origin of time, thus making possible to assume that $\phi = \phi_V$ and hence obtain simpler relationships. These are summarized in the main text as Eqs. (6)–(9).

A.2. *Multi-reach approach*

The multi-reach approach divides the whole channel into sub-sections. In each sub-section, the solutions for four unknown complex numbers $a_1^*, a_2^*, w_1^*, w_2^*$ are obtained by solving a set of linear equations satisfying the internal boundary conditions (i.e. continuity of water level and discharge) at the junctions of these sub-reaches [see details in Toffolon and Savenije, 2011]. Specifically, we evaluated the main tidal dynamics at the seaward boundary of each sub-section (i.e. $x^* = 0$) by moving the origin axis, thus it directly follows from (A.2), (A.8) and (A.9) that the amplification number δ_A and the celerity number λ_A are given by:

$$\delta_A = \Re\left(\frac{a_1^* w_1^* + a_2^* w_2^*}{a_1^* + a_2^*}\right), \tag{A.18}$$

$$\lambda_A = -\Im\left(\frac{a_1^* w_1^* + a_2^* w_2^*}{a_1^* + a_2^*}\right). \tag{A.19}$$

With obtained δ_A and λ_A, the rest of dependent parameters δ_V, λ_V, ϕ and μ can be computed from Eqs. (6), (7), (9) and (10). The longitudinal dimensional tidal amplitude can be reproduced by $\eta = \zeta_0 \overline{h}|a_1^* + a_2^*|$, while the longitudinal dimensional velocity amplitude can be computed according to the definition of the velocity number μ (see Table 1) and is given by $\upsilon = \mu r_S \zeta c_0$. An example of Matlab scripts is provided as supplement to illustrate the computation process.

Appendix B. Tidal Dynamics in an Infinite Channel

An infinite channel is characterized by a length L^* approaching infinity. Then, $a_1^* = 0$ in (A.10), and the set of Eqs. (6), (7), (8), (9) and (A.13) can be rewritten as:

$$\delta_V = \delta_A = \frac{1}{2}\gamma - \frac{1}{4}\sqrt{2m - 8 + 2\gamma^2}, \tag{B.1}$$

$$\lambda_V^2 = \lambda_A^2 = \frac{1}{8}m + \frac{1}{2} - \frac{1}{8}\gamma^2, \tag{B.2}$$

$$\mu^2 = \frac{1}{4}\frac{\gamma^2 - \gamma\sqrt{2m - 8 + 2\gamma^2} + m}{1 + \widehat{\chi}^2}, \tag{B.3}$$

$$\tan(\phi) = \frac{2\gamma + \sqrt{2m - 8 + 2\gamma^2}}{\sqrt{2m + 8 - 2\gamma^2}}, \tag{B.4}$$

with $m = \sqrt{16 - 8\gamma^2 + \gamma^4 + 16\widehat{\chi}^2}$. These equations correspond to the analytical results for an infinite channel without reflected wave [see also Toffolon and Savenije, 2011]. However, the set of Eqs. (B.1)–(B.4) is still implicit since $\widehat{\chi}$ contains an *a priori* unknown μ describing the dimensionless scale of velocity.

Simpler relationships between these main tidal dynamics were provided by Cai *et al.* [2012] using the 'envelope method', where a tidal damping equation is obtained by subtracting the envelope curves of high water and low water. Making use of Lorentz's linearization for the quadratic velocity [Lorentz, 1926], Cai *et al.* [2012] shows that the tidal wave propagation in an infinite channel can be described by a set of four implicit equations, i.e. the damping equation, the celerity equation, the scaling equation and the phase lag equation:

$$\delta_V = \delta_A = \frac{\gamma}{2} - \frac{4}{3\pi}\frac{\chi\mu}{\lambda_A}, \tag{B.5}$$

$$\lambda_V^2 = \lambda_A^2 = 1 - \delta_A(\gamma - \delta_A), \tag{B.6}$$

$$\mu = \frac{\cos(\phi)}{\lambda_A} = \frac{\sin(\phi)}{\delta_A - \gamma}, \tag{B.7}$$

$$\tan(\phi) = \frac{\delta_A - \gamma}{\lambda_A}. \tag{B.8}$$

This system can be solved by a simple Newton–Raphson method.

Appendix C. Analytical Solution for Resonance in Frictionless Channels

C.1. *Subcritical convergence*

The subcritical case is characterized by $\gamma < 2$, hence $\Lambda = i\sqrt{1 - (\gamma/2)^2}$. Thus, the right hand side of Eq. (A.13) can be separated into its real and imaginary parts,

where the imaginary part is $\lambda_A = 0$, and the real part provides

$$\delta_A = \frac{\sin(2\pi\alpha L^*)}{\cos(2\pi\alpha L^* - \theta) + \alpha/2}, \tag{C.1}$$

with $\alpha = \sqrt{4-\gamma^2} = -2i\Lambda$ and $\theta = \arccos(\alpha/2)$.

We can obtain the position of the antinodes by setting $\delta_A = 0$ in Eq. (C.1). This correspond to the condition that the numerator of (C.1) is zero, which provides the solution $L^* = n/(2\alpha)$, where $n = 0, 1, 2, \ldots$ is a positive integer number (we use the same notation in the following expressions). The position of the nodes is more difficult to define because it should be obtained by setting $\eta = 0$, while we have an equation for δ_A. However, we can exploit the fact that the sign of δ_A changes in a node, which represents a discontinuity. This condition can be obtained by setting the denominator of (C.1) equal to zero, which provides two solutions. The first solution is given by the values $L^* = (1+2n)/(2\alpha)$, which is composed by odd multiples of $1/(2\alpha)$ that were already included in the solutions obtained for the antinodes. In these positions the ratio is theoretically indefinite (0/0), but δ_A assumes a finite value and is continuous, so these values must be excluded from the solutions for the antinodes, which are located only in the even multiples of $1/(2\alpha)$. The second solution obtained for the nodes does not overlap with that of the antinodes, and hence represents the actual set of values for the positions of the nodes. Hence, the position of nodes and antinodes in a frictionless channel can be summarized as follows:

$$L^{*A}_{\text{antinode}} = \frac{n}{\alpha}, \tag{C.2}$$

$$L^{*A}_{\text{node}} = \frac{\arccos(\alpha/2)}{\pi\alpha} + \frac{2n+1}{2\alpha}. \tag{C.3}$$

A simple relationship for the tidal damping for velocity can be obtained from (6) in the case without friction:

$$\delta_V = \gamma - \frac{1}{\delta_A}. \tag{C.4}$$

Moreover, Eq. (8) directly yields $\mu = \delta_A$. The positions of the velocity amplitude nodes and antinodes can be computed using the conditions $\upsilon = 0$ (whereby $\mu = \delta_A = 0$) and $\delta_V = 0$, respectively:

$$L^{*V}_{\text{node}} = L^{*A}_{\text{antinode}} = \frac{n}{\alpha}, \tag{C.5}$$

$$L^{*V}_{\text{antinode}} = -\frac{\arccos(\alpha/2)}{\pi\alpha} + \frac{2n+1}{2\alpha}. \tag{C.6}$$

In a prismatic channel, we can set $\gamma = 0$ (hence $\alpha = 2$) and obtain the well–known solution $L^{*A}_{\text{node}} = L^{*V}_{\text{antinode}} = (2n+1)/4$ and $L^{*A}_{\text{antinode}} = L^{*V}_{\text{node}} = n/2$. The classical quarter wavelength resonance then occurs when the tidal period coincides with the

resonance period $T_{r0} = 4L_e/[c_0(2n+1)]$. Recalling that $\mu = \delta_A$ and using (C.1) with $\gamma = 0$, it follows that

$$\mu|_{\gamma=0} = \frac{\sin(4\pi L^*)}{\cos(4\pi L^*) + 1} = \tan(2\pi L^*), \tag{C.7}$$

from which the velocity amplitude υ can be calculated according to the definition in Table 1. For short prismatic channels (i.e. $2\pi L^* \ll 1$), it directly follows that the velocity increases approximately linearly with the length.

C.2. *Supercritical convergence*

In the case of supercritical convergence in a frictionless estuary ($\gamma \geq 2$, $\widehat{\chi} = 0$), then $\Lambda = \sqrt{(\gamma/2)^2 - 1}$ is a real number. Similar to the previous case, algebraic manipulation allows one to separate the real and imaginary parts of Eq. (A.13). The result is that $\lambda_A = 0$ (i.e. a standing wave with infinite celerity) and

$$\delta_A = \frac{\gamma}{2} - \Lambda \left[1 - \frac{2}{1 + \exp(4\pi\Lambda L^*)\frac{\Lambda+\gamma/2}{\Lambda-\gamma/2}} \right], \tag{C.8}$$

which is always positive, indicating that in strongly convergent estuaries the tidal amplitude always increases along the estuary axis. An example of the solution in this case is given in Figs. 4(b) and 4(d).

It is worth noting that $(4\pi\Lambda)^{-1}$ defines a characteristic dimensionless length scale. If the distance $L^* \gg (4\pi\Lambda)^{-1}$, the denominator in the last term of Eq. (C.8) goes to infinity, which leads to an equilibrium value of $\delta_A = \gamma/2 - \Lambda = \gamma/2 - \sqrt{\gamma^2/4 - 1}$ far from the channel head, thus tending to the case of an infinite estuary described by Eq. (56) of Savenije *et al.* [2008]. In this case, the amplification decreases with increasing convergence [see also Fig. 4(d)], as can be seen by rearranging the above relationship and evaluating the limit $\delta_A = (\gamma/2 + \sqrt{\gamma^2/4 - 1})^{-1} \to \gamma^{-1}$ for $\gamma \gg 2$.

We note that neither nodes nor antinodes for tidal amplitude exist in this case. There only exists a single node for the velocity amplitude at the head of an estuary ($L^{*V}_{\text{node}} = 0$). The position of the velocity amplitude antinode can be determined by setting $\delta_V = 0$ in Eq. (C.4) in combination with Eq. (C.8) to obtain

$$L^{*V}_{\text{antinode}} = \frac{1}{4\pi\Lambda} \ln\left(\frac{\gamma + 2\Lambda}{\gamma - 2\Lambda}\right). \tag{C.9}$$

The position L^{*V}_{antinode} decreases as γ increases, hence bringing the maximum of velocity amplitude closer to the head of the estuary in strongly convergent estuaries. It is interesting to note that Eq. (C.6) (subcritical) and (C.9) (supercritical) are continuous (see Fig. 5), being $L^{*V}_{\text{antinode}} = (2\pi)^{-1}$ the position of the first antinode when $\gamma = 2$.

Appendix D. Interaction Between Dominant and Weaker Tidal Constituents

In this Appendix, we propose a simple conceptual model illustrating the nonlinear interaction between dominant and weaker tidal constituents. For simplicity, we assume that the tidal current is composed of one dominant constituent (e.g. M_2) with velocity U_1, and a weaker constituent (e.g. S_2) with velocity U_2:

$$U = U_1 + U_2 = \upsilon_1 \cos(\omega_1 t) + \upsilon_2 \cos(\omega_2 t) = \upsilon_1[\cos(\omega_1 t) + \epsilon \cos(\omega_2 t)], \quad \text{(D.1)}$$

where $\epsilon = \upsilon_2/\upsilon_1$, with υ_1, υ_2 the velocity amplitudes of the first and second constituent, and ω_1 and ω_2 their frequencies. We assume the second component is actually minor with respect to the dominant ($\epsilon \ll 1$).

The Fourier expansion of $U|U|$ can be written as [e.g. Fang, 1987; Inoue and Garrett, 2007]:

$$U|U| = \frac{8}{3\pi}\upsilon_1(\beta_1 U_1 + \beta_2 U_2), \quad \text{(D.2)}$$

where β_1 and β_2 are the Fourier coefficients that account for the nonlinear interaction between dominant M_2 and weaker tidal component S_2. The fourth-order approximations of β_1 and β_2 are given by [see Fang, 1987; Inoue and Garrett, 2007]:

$$\beta_1 = 1 + \frac{3}{4}\epsilon^2 - \frac{3}{64}\epsilon^4 + O(\epsilon^6), \quad \text{(D.3)}$$

$$\beta_2 = \frac{3}{2}\left(1 + \frac{1}{8}\epsilon^2 + \frac{1}{192}\epsilon^4\right) + O(\epsilon^6). \quad \text{(D.4)}$$

Combining Eqs. (3), (4) and (D.2), and neglecting the nonlinear advective terms, yields

$$\frac{\partial U_1}{\partial t} + \frac{\partial U_2}{\partial t} + g\frac{\partial Z_1}{\partial x} + g\frac{\partial Z_2}{\partial x} + \frac{8}{3\pi}\frac{g\upsilon_1}{K^2\overline{h}^{4/3}}(\beta_1 U_1 + \beta_2 U_2) = 0, \quad \text{(D.5)}$$

where Z_1 is the free surface elevation for the dominant constituent while Z_2 for the secondary constituent. Exploiting the linearity of Eq. (D.5), we can solve the two problems independently.

We separate the equation for the dominant component:

$$\frac{\partial U_1}{\partial t} + g\frac{\partial Z_1}{\partial x} + r_1 U_1 = 0, \quad \text{(D.6)}$$

where $r_1 = \frac{8}{3\pi}\frac{g\upsilon_1}{K^2\overline{h}^{4/3}}\beta_1$ is the effective linearized friction term. By comparing it with the coefficient r defined in Eq. (5), i.e. when dealing with only one single tidal constituent, the effect of the simultaneous presence of the S_2 tidal component on the dominant M_2 yields a correction factor β_1. By referring to Eq. (D.3), the assumption $\epsilon \ll 1$ implies that $\beta_1 \simeq 1$, suggesting the obvious result that a very weak secondary component does not significantly alter the dominant one.

The remaining terms of Eq. (D.5) can be related to the second tidal constituent:

$$\frac{\partial U_2}{\partial t} + g\frac{\partial Z_2}{\partial x} + \widehat{r_2}U_2 = 0. \tag{D.7}$$

It directly follows from the comparison of (D.5), (D.6) and (D.7) that $\widehat{r_2} = \frac{8}{3\pi}\frac{g\upsilon_1}{K^2\overline{h}^{4/3}}\beta_2$. In order to treat Eq. (D.7) for the secondary component as the 'normal' case of a single tidal constituent, we would have to introduce a correction factor f such that

$$\frac{\partial U_2}{\partial t} + g\frac{\partial Z_2}{\partial x} + fr_2U_2 = 0, \tag{D.8}$$

with $r_2 = \frac{8}{3\pi}\frac{g\upsilon_2}{K^2\overline{h}^{4/3}}$. Consequently, the estimate of the correction factor for the secondary constituent for S_2 reads:

$$f = \frac{\widehat{r_2}}{r_2} = \frac{\upsilon_1}{\upsilon_2}\beta_2 = \frac{\beta_2}{\epsilon}. \tag{D.9}$$

Equation (D.9) suggests that f grows with decreasing ϵ, so a weak secondary component will be characterized by large values of f.

The above procedure can easily be extended to examine the situation with more than two constituents, which is the case in real estuaries.

Acknowledgments

We acknowledge the financial support from the National Key Research Programme of China (Grant No. 2016YFC0402600), from the National Natural Science Foundation of China (Grant No. 41476073) and from the Water Resource Science and Technology Innovation Program of Guangdong Province (Grant No. 2016-20).

References

Alebregtse, N. C. & de Swart, H. E. [2014] "Effect of a secondary channel on the non-linear tidal dynamics in a semi-enclosed channel: A simple model," *Ocean Dynam.* **64**(4), 573–585, doi:10.1007/s10236-014-0690-0.

Alebregtse, N. C., de Swart, H. E. & Schuttelaars, H. M. [2013] "Resonance characteristics of tides in branching channels," *J. Fluid Mech.* **728**, doi:10.1017/Jfm.2013.319.

Bennett, A. F. [1975] "Tides in bristol channel," *Geophys. J. Roy. Astr. S.* **40**(1), 37–43, doi:10.1111/j.1365-246X.1975.tb01604.x.

Cai, H. [2014] "A new analytical framework for tidal propagation in estuaries", Ph.D. Thesis, Delft University of Technology, Delft, the Netherlands, doi:10.4233/uuid:b3e7f2ab-b250-40ab-a353-d71377b6b73d, Available at http://repository.tudelft.nl/view/ir/uuid:b3e7f2ab-b250-40ab-a353-d71377b6b73d/ (last access 24 Nov. 2015).

Cai, H., Savenije, H. H. G. & Toffolon, M. [2012] "A new analytical framework for assessing the effect of sea-level rise and dredging on tidal damping in estuaries," *J. Geophys. Res.* **117**(C09023), doi:10.1029/2012JC008000.

Cai, H., Toffolon, M. & Savenije, H. H. G. [2015] "Analytical investigation of superposition between predominant M2 and other tidal constituents in estuaries," in *Proceedings of 36th IAHR World Congress* (Delft–The Hague), pp. 1–4.

Cerralbo, P., Grifoll, M., Valle-Levinson, A. & Espino, M. [2014] "Tidal transformation and resonance in a short, microtidal Mediterranean estuary (Alfacs Bay in Ebre delta)," *Estuar. Coast Shelf S.* **145**, 57–68, doi:10.1016/j.ecss.2014.04.020.

Chernetsky, A. S., Schuttelaars, H. M. & Talke, S. A. [2010] "The effect of tidal asymmetry and temporal settling lag on sediment trapping in tidal estuaries," *Ocean Dynam.* **60**(5), 1219–1241, doi:10.1007/s10236-010-0329-8.

Diez-Minguito, M., Baquerizo, A., Ortega-Sanchez, M., Navarro, G. & Losada, M. A. [2012] "Tide transformation in the Guadalquivir estuary (SW Spain) and process-based zonation," *J. Geophys. Res.* **117**(C03019), doi:10.1029/2011jc007344.

Ensing, E., de Swart, H. E. & Schuttelaars, H. M. [2015] "Sensitivity of tidal motion in well-mixed estuaries to cross-sectional shape, deepening, and sea level rise," *Ocean Dynam.* **65**(7), 933–950, doi:10.1007/s10236-015-0844-8.

Fang, G. [1987] "Nonlinear effects of tidal friction," *Acta Oceanologica Sin.* **6 (Suppl.)**(1), 105–122.

Fong, S. W. & Heaps, N. S. [1978] "Note on quarter-wave tidal resonance in the Bristol Channel," Technical Report, Institute of Oceanographic Sciences.

Friedrichs, C. T. [2010] "Barotropic tides in channelized estuaries," A. Valle-Levinson (ed.), *Contemporary Issues in Estuarine Physics* (Cambridge University Press, Cambridge, UK), pp. 27–61.

Friedrichs, C. T. & Aubrey, D. G. [1994] "Tidal propagation in strongly convergent channels," *J. Geophys. Res.* **99**(C2), 3321–3336, doi:10.1029/93jc03219.

Garcia-Lafuente, J., Delgado, J., Navarro, G., Calero, C., Diez-Minguito, M., Ruiz, J. & Sanchez-Garrido, J. C. [2012] "About the tidal oscillations of temperature in a tidally driven estuary: The case of guadalquivir estuary, Southwest Spain," *Estuar. Coast Shelf S.* **111**, 60–66.

Garrett, C. [1972] "Tidal resonance in the Bay of Fundy and Gulf of Maine," *Nature* **238**, 441–443, doi:10.1038/238441a0.

Godin, G. [1988] "The resonant period of the Bay of Fundy," *Cont. Shelf Res.* **8**, 1005–1010, doi:10.1016/0278-4343(88)90059-3.

Godin, G. [1993] "On tidal resonance," *Cont. Shelf Res.* **13**(1), 89–107, doi:10.1016/0278-4343(93)90037-X.

Greenberg, D. A. [1979] "A numerical model investigation of tidal phenomena in the Bay of Fundy and Gulf of Maine," *Marine Geodesy* **2**(2), 161–187, doi:10.1080/15210607909379345.

Hunt, J. N. [1964] "Tidal oscillations in estuaries," *Geophys. J. Roy. Astr. S.* **8**(4), 440–455, doi:10.1111/j.1365-246X.1964.tb03863.x.

Ianniello, J. P. [1979] "Tidally induced residual currents in estuaries of variable breadth and depth," *J. Phys. Oceanogr.* **9**(5), 962–974, doi:10.1175/1520-0485(1979)009⟨0962:Tircie⟩2.0.Co;2.

Inoue, R. & Garrett, C. [2007] "Fourier representation of quadratic friction," *J. Phys. Oceanogr.* **37**(3), 593–610, doi:10.1175/Jpo2999.1.

Ippen, A. T. [1966] "Tidal dynamics in estuaries, part I: Estuaries of rectangular section," *Estuary and Coastline Hydrodynamics*, ed. Ippen, A. T. (McGraw-Hill, New York), pp. 493–545.

Jay, D. A. [1991] "Green law revisited - tidal long-wave propagation in channels with strong topography," *J. Geophys. Res.* **96**(C11), 20585–20598, doi:10.1029/91jc01633.

Jiang, W. S. & Feng, S. Z. [2014] "3d analytical solution to the tidally induced Lagrangian residual current equations in a narrow bay," *Ocean Dynam.* **64**(8), 1073–1091, doi:10.1007/s10236-014-0738-1.

Ku, D. A., L. F. and Greenberg, Garrett, C. J. R. & Dobson, F. W. [1985] "Nodal modulation of the lunar semidiurnal tide in the Bay of Fundy and the Gulf of Maine," *Sciences* **230**, 69–71, doi:10.1126/science.230.4721.69.

Lanzoni, S. & Seminara, G. [1998] "On tide propagation in convergent estuaries," *J. Geophys. Res.* **103**(C13), 30793–30812, doi:10.1029/1998JC900015.

Li, C. Y. & Valle-Levinson, A. [1999] "A two-dimensional analytic tidal model for a narrow estuary of arbitrary lateral depth variation: The intratidal motion," *J. Geophys. Res.* **104**(C10), 23525–23543, doi:10.1029/1999jc900172.

Liang, D. F., Xia, J. Q., Falconer, R. A. & Zhang, J. X. [2014] "Study on tidal resonance in Severn Estuary and Bristol Channel," *Coast Eng. J.* **56**(1), doi:10.1142/S0578563414500028.

Lorentz, H. A. [1926] "Verslag staatscommissie zuiderzee (in dutch)," Technical Report, Alg. Landsdrukkerij.

Pingree, R. D. [1983] "Spring tides and quadratic friction," *Deep-Sea Res. A — Oceanographic Research Papers* **30**(9), 929–944, doi:10.1016/0198-0149(83)90049-3.

Prandle, D. [1985] "Classification of tidal response in estuaries from channel geometry," *Geophys. J. Roy. Astr. S.* **80**(1), 209–221, doi:10.1111/j.1365-246X.1985.tb05086.x.

Prandle, D. [2003] "Relationships between tidal dynamics and bathymetry in strongly convergent estuaries," *J. Phys. Oceanogr.* **33**(12), 2738–2750.

Prandle, D. & Rahman, M. [1980] "Tidal response in estuaries," *J. Phys. Oceanogr.* **10**(10), 1552–1573, doi:10.1175/1520-0485(1980)010⟨1552:TRIE⟩2.0.CO;2.

Rainey, R. C. T. [2009] "The optimum position for a tidal power barrage in the Severn estuary," *J. Fluid Mech.* **636**, 497–507, doi:10.1017/S0022112009991443.

Robinson, I. S. [1980] "Tides in the Bristol Channel - an analytical wedge model with friction," *Geophys. J. Roy. Astr. S.* **62**(1), 77–95, doi:10.1111/j.1365-246X.1980.tb04845.x.

Roos, P. C. & Schuttelaars, H. M. [2011] "Influence of topography on tide propagation and amplification in semi-enclosed basins," *Ocean Dynam.* **61**(1), 21–38, doi:10.1007/s10236-010-0340-0.

Roos, P. C., Velema, J. J., Hulscher, S. J. M. H. & Stolk, A. [2011] "An idealized model of tidal dynamics in the North Sea: Resonance properties and response to large-scale changes," *Ocean Dynam.* **61**(12), 2019–2035, doi:10.1007/s10236-011-0456-x.

Savenije, H. H. G. [2005] *Salinity and Tides in Alluvial Estuaries* (Elsevier, New York).

Savenije, H. H. G. [2012] *Salinity and Tides in Alluvial Estuaries* (2nd completely revised edition), Available at: www.salinityandtides.com accessed on 26 December 2014.

Savenije, H. H. G., Toffolon, M., Haas, J. & Veling, E. J. M. [2008] "Analytical description of tidal dynamics in convergent estuaries," *J. Geophys. Res.* **113**(C10025), doi:10.1029/2007JC004408.

Schuttelaars, H. M., de Jonge, V. N. & Chernetsky, A. [2013] "Improving the predictive power when modelling physical effects of human interventions in estuarine systems," *Ocean Coastal Manage.* **79**, 70–82, doi:10.1016/j.ocecoaman.2012.05.009.

Souza, A. J. & Hill, A. E. [2006] "Tidal dynamics in channels: Single channels," *J. Geophys. Res.* **111**(C9), doi:10.1029/2006jc003469.

Taylor, G. I. [1921] "Tides in the bristol channel," *P. Camb. Philos. Soc.* **20**, 320–325.

Toffolon, M. & Savenije, H. H. G. [2011] "Revisiting linearized one-dimensional tidal propagation," *J. Geophys. Res.* **116**(C07007), doi:10.1029/2010JC006616.

Toffolon, M., Vignoli, G. & Tubino, M. [2006] "Relevant parameters and finite amplitude effects in estuarine hydrodynamics," *J. Geophys. Res.* **111**(C10014), doi:10.1029/2005JC003104.

van Rijn, L. C. [2011] "Analytical and numerical analysis of tides and salinities in estuaries; part I: Tidal wave propagation in convergent estuaries," *Ocean Dynam.* **61**(11), 1719–1741, doi:10.1007/s10236-011-0453-0.

Wang, Z. B., Winterwerp, J. C. & He, Q. [2014] "Interaction between suspended sediment and tidal amplification in the Guadalquivir estuary," *Ocean Dynam.* **64**(10), 1487–1498, doi:10.1007/s10236-014-0758-x.

Waterhouse, A. F., Valle-Levinson, A. & Winant, C. D. [2011] "Tides in a system of connected estuaries," *J. Phys. Oceanogr.* **41**(5), 946–959, doi:10.1175/2010jpo4504.1.

Webb, D. J. [2012] "On the shelf resonances of the Gulf of Carpentaria and the Arafura Sea," *Ocean Sci.* **8**, 733–750, doi:10.5194/os-8-733-2012.

Webb, D. J. [2013] "On the shelf resonances of the English Channel and Irish Sea," *Ocean Sci.* **9**, 731–744, doi:10.5194/os-9-731-2013.

Webb, D. J. [2014] "On the tides and resonances of Hudson Bay and Hudson Strait," *Ocean Sci.* **10**, 411–426, doi:10.5194/os-10-411-2014.

Winant, C. D. [2007] "Three-dimensional tidal flow in an elongated, rotating basin," *J. Phys. Oceanogr.* **37**(9), 2345–2362, doi:10.1175/Jpo3122.1.

Winterwerp, J. C. & Wang, Z. B. [2013] "Man-induced regime shifts in small estuaries-I: Theory," *Ocean Dynam.* **63**(11–12), 1279–1292, doi:10.1007/s10236-013-0662-9.

Xia, J. Q., Falconer, R. A. & Lin, B. L. [2010] "Impact of different tidal renewable energy projects on the hydrodynamic processes in the Severn Estuary, UK," *Ocean Model.* **32**(1–2), 86–104, doi:10.1016/j.ocemod.2009.11.002.

Zhong, L. J., Li, M. & Foreman, M. G. G. [2008] "Resonance and sea level variability in Chesapeake bay," *Cont. Shelf Res.* **28**(18), 2565–2573, doi:10.1016/j.csr.2008.07.007.

Zhou, J. T., Pan, S. Q. & Falconer, R. A. [2014] "Effects of open boundary location on the far-field hydrodynamics of a Severn Barrage," *Ocean Model.* **73**, 19–29, doi:10.1016/j.ocemod.2013.10.006.

Zimmerman, J. T. F. [1982] "On the Lorentz linearization of a quadratically damped forced oscillator," *Phys. Lett. A* **89**(3), 123–124, doi:10.1016/0375-9601(82)90871-4.